MRCKα is activated by caspase cleavage to assemble an apical actin ring for epithelial cell extrusion

Paolo Armando Gagliardi,[1,2] Desiana Somale,[1,2] Alberto Puliafito,[2] Giulia Chiaverina,[1,2] Laura di Blasio,[1,2] Michele Oneto,[3] Paolo Bianchini,[3] Federico Bussolino,[1,2] and Luca Primo[1,2]

[1]Department of Oncology, University of Torino, Turin, Italy
[2]Candiolo Cancer Institute, Fondazione del Piemonte per l'Oncologia, Istituto di Ricovero e Cura a Carattere Scientifico, Candiolo, Italy
[3]Nanoscopy, Istituto Italiano di Tecnologia, Genoa, Italy

Extrusion of apoptotic cells from epithelial tissues requires orchestrated morphological rearrangements of the apoptotic cell and its neighbors. However, the connections between the apoptotic cascade and events leading to extrusion are not fully understood. Here, we characterize an apoptotic extrusion apical actin ring (EAAR) that is assembled within the apoptotic cell and drives epithelial extrusion. Caspase-mediated cleavage of myotonic dystrophy kinase–related CDC42-binding kinase-α (MRCKα) triggers a signaling pathway that leads to the assembly of EAAR that pulls actin bundles, resulting in the compaction and removal of the cell body. We provide a detailed portrait of the EAAR including F-actin flow, the contribution of myosin contraction, and actin polymerization at bundles' terminals when the product of MRCKα cleavage is expressed. These results add to our understanding of the mechanisms controlling the process of epithelial extrusion by establishing a causal relationship between the triggering events of apoptosis, the activation of MRCKα, and its subsequent effects on the dynamics of actomyosin cytoskeleton rearrangement.

Introduction

Epithelial layers self-control their homeostatic state by precise removal of aged or critically compromised cells, compensated by fast replication rates. Epithelial homeostasis is indeed critically required for proper maintenance of barrier, defense, and transport functions of all epithelia. Loss of epithelial homeostasis is, on the other hand, associated with different pathological events, including cancer (Macara et al., 2014).

To efficiently remove dying cells from epithelia, multicellular organisms have evolved epithelial extrusion. During this process, actomyosin rearrangements occurring in both apoptotic and neighboring cells allow apoptotic cells to be expelled without leaving unfilled space (Rosenblatt et al., 2001; Kuipers et al., 2014; Wu et al., 2015). To obtain this goal, extruding epithelial cells must coordinate with the neighboring ones. Along this line, it was discovered that S1P is the mediator used by apoptotic cells to communicate their status to their neighbors, which in turn assemble a basal actomyosin constriction ring (Gu et al., 2011). Less investigated. however, is the morphological and mechanical role of apoptotic cells themselves during epithelial extrusion.

Apoptosis is triggered by at least three alternative pathways (intrinsic, extrinsic, and perforin/granzyme pathways), which all converge into the cascade of caspases (Elmore, 2007; Cullen and Martin, 2009). These cysteine-proteases specifically hydrolyze a peptide bond in the C terminus to specific aspartate residues in their substrates (Black et al., 1989) and drive the

irreversible events of apoptosis, including activation of cytoplasmic endonucleases, cytoskeleton rearrangements, and formation of bleb and apoptotic bodies (Crawford and Wells, 2011).

Most of the morphological events associated with apoptosis are governed by the actomyosin cytoskeleton. Indeed, myosin contraction is required for nuclear fragmentation (Croft et al., 2005), apoptotic body formation (Coleman et al., 2001), and release of immunomodulatory molecules by a limited membrane permeabilization (Wickman et al., 2013). However, despite the importance of the actomyosin cytoskeleton in apoptosis, how it is regulated is far from fully understood. Still controversial is the role of caspase-mediated cleavage of actin (Rice et al., 1998; Mashima et al., 1999) and of the actin-severing protein gelsolin (Kothakota et al., 1997), which was reported to determine actin cytoskeleton disassembly and cellular rounding up. More relevant is instead the regulation of myosin contraction. Rho-associated protein kinase 1 (ROCK1) kinase activity on myosin light chain 2 (MLC2), the regulatory subunit of nonmuscular myosin, is potently increased upon proteolytic cleavage by caspase 3. This event causes contraction of the cortical actomyosin network and thereby determines bleb formation (Coleman et al., 2001; Sebbagh et al., 2001).

ROCK1 belongs to a small subgroup of AGC serine/threonine kinases sharing the ability to phosphorylate MLC2. This

Correspondence to Luca Primo: luca.primo@unito.it; Paolo Armando Gagliardi: paolo.gagliardi@izb.unibe.ch

subgroup, in addition to ROCK1, includes ROCK2, myotonic dystrophy kinase–related CDC42-binding kinase-α (MRCKα), MRCKβ, MRCKγ, citron Rho-interacting kinase, and myotonin protein kinase (DMPK; Pearce et al., 2010). With the exception of ROCK2, which is activated only by granzyme B–mediated proteolytic cleavage (Sebbagh et al., 2005), the role in the apoptotic process of these kinases has never been investigated.

Here we describe the discovery of MRCKα as a downstream effector of apoptosis and trigger of epithelial extrusion. MRCKα was previously described as an important regulator of cytoskeletal dynamics (Leung et al., 1998; Tan et al., 2008) and related processes, such as nuclear movement, microtubule-organizing center polarization (Gomes et al., 2005), and protrusion dynamics (Gagliardi et al., 2014; Lee et al., 2014). Beyond the space- and time-restricted roles in normal cell life, we report that MRCKα is constitutively activated by proteolytic cleavage at aspartate 478, causing an increase of its kinase activity on MLC2. During epithelial extrusion, MRCKα activation determines the formation of one extrusion apical actin ring (EAAR) in each apoptotic cell. This actomyosin structure is in turn responsible for the production of cell-autonomous forces in the early events of epithelial extrusion. We therefore provide evidence that the apoptotic cell autonomously contributes to the execution of epithelial cell extrusion by activating MRCKα.

Results

Assembly of apoptotic extrusion apical actin ring (aEAAR) drives actomyosin rearrangements within the extruding cell

To investigate actin cytoskeleton rearrangement during cell extrusion, we performed time-lapse microscopy on extrusion events occurring in confluent MCF10A epithelia labeled with LifeAct-EGFP or LifeAct-Ruby markers (Video 1). During cell extrusion, both the extruding cell itself and its neighbors show profound and progressive actin cytoskeleton modifications (Fig. 1 A and Video 2). In particular, we observed (a) an apical actin ring (here termed as aEAAR to distinguish it from the iEAAR experimentally induced by cleaved MRCKα expression) formed within the extruding cell; and (b) a basal actin ring formed by the boundaries between the extruding cell and its neighbors. These events are not synchronous, as the completion of aEAAR assembly always comes first and is then followed by constriction of the basal ring (Fig. 1 B). In all cases, the formation of aEAAR is preceded by cortical contraction of the apical side (Fig. S1 A). Upon assembly, the aEAAR is associated with multiple and dynamic actin bundles (Fig. S1 B). The same sequence of events was observed in MDCK undergoing epithelial extrusion (Fig. S1 C).

The assembly aEAAR is a dynamic process in which we recognized four objectively identifiable phases: (1) cortical actin contraction; (2) thickening of F-actin in some patches; (3) connections of F-actin patches by F-actin bundles; and (4) coalescence of all patches in a single ring-shaped F-actin structure (Fig. 1, C and D; and Video 3).

From a structural point of view, the aEAAR is a 3D thick structure, connected to multiple actin bundles (Fig. 1 E). The outer shape is circular, and fluorescence intensity profiles reveal a hollow inner core, devoid of F-actin fluorescence signal, whereas the outer part is highly fluorescing. Statistical analysis of radial F-actin distribution revealed that the higher F-actin

density occurs at 0.7721 ± 0.1278 µm from aEAAR center, whereas the half decay of F-actin is distributed at 1.4977 ± 0.1708 µm from aEAAR center (Fig. 1 F).

Apoptotic epithelial extrusion is controlled by myosin contraction and MRCKα

The presence of an apical F-actin ring in the extruding epithelial cells suggests a prominent role for cell-autonomous cytoskeletal rearrangements. We quantified the rate of extrusion induced in MCF10A cells by growth factor deprivation by counting the fraction of cells released from a confluent layer in 16 h. We found that the rate of extrusion upon growth factor deprivation was about fivefold higher than in control cells (Fig. 2 A). By live imaging, we observed that both formation of aEAAR and cell extrusion are associated with caspase activation, highlighting the execution of an apoptotic extrusion program (Fig. S2 A). To understand the contribution of programmed cell death on total extrusion events, we treated cells with the tBid inhibitor BI-6C9 and the pan-caspase inhibitor z-VAD-FMK. Treatment with the two drugs resulted in a severe reduction of extruded cells, proving that caspase-dependent programmed cell death accounts for the majority of extrusion events (Fig. 2, B and C). As previously described (Rosenblatt et al., 2001), contractile forces generated by actomyosin activity are the main mechanical executors of cell extrusion, and indeed, in our experiments, the use of the myosin inhibitor blebbistatin hampered the effect of growth factor deprivation (Fig. 2 D).

Cell extrusion requires a concerted action between the apoptotic cell and the neighbors in the formation and contraction of a basal actomyosin ring (Rosenblatt et al., 2001). However, spatio-temporal dynamics of the actin cytoskeleton revealed the existence of a cell-autonomous, myosin-dependent component activated by the apoptotic signaling cascade during epithelial extrusion (Fig. 1, A and B). Because nonmuscular myosin activity is regulated by phosphorylation of MLC2 by proteins of the Rho kinase family, we wondered whether apoptotic signals might activate members of this group of kinases. It has been previously shown that active caspase 3 cleaves ROCK1 and removes its inhibitory domain, thereby producing a constitutively active truncated kinase (Coleman et al., 2001; Sebbagh et al., 2001). A similar mechanism of activation has not yet been described for other Rho kinase family members despite their structural homology and shared ability to phosphorylate MLC2.

We investigated whether ROCK1 and other family members were involved in the process of cell extrusion. DMPK and MRCKγ were excluded from further analysis, as they are not expressed in MCF10A cells (Fig. S2 B). Based on our in silico analysis, we further excluded CIT and ROCK2, which do not have potential caspase cleavage sites (Fig. S2 C). Accordingly, ROCK2 was not cleaved by caspases in cells during apoptosis (Fig. S2 D), although exogenous overexpression of a truncated form of ROCK2 was shown to induce epithelial extrusion (Lubkov and Bar-Sagi, 2014).

Therefore, we focused on ROCK1, which has already been shown to be involved in caspase-dependent membrane blebbing (Sebbagh et al., 2001), MRCKα, and MRCKβ (Fig. S2 E). We evaluated the role of these proteins in epithelial extrusion by stable silencing of MCF10A cells with a pair of lentiviral vectors encoding shRNAs for each protein (Fig. 2 E). We found that the silencing of MRCKα was able to significantly blunt apoptotic epithelial extrusion, whereas the silencing of ROCK1 and MRCKβ was largely ineffective (Fig. 2 F). MRCKα silencing did not result in an impairment of apoptosis but instead led to a deficiency of cell extrusion,
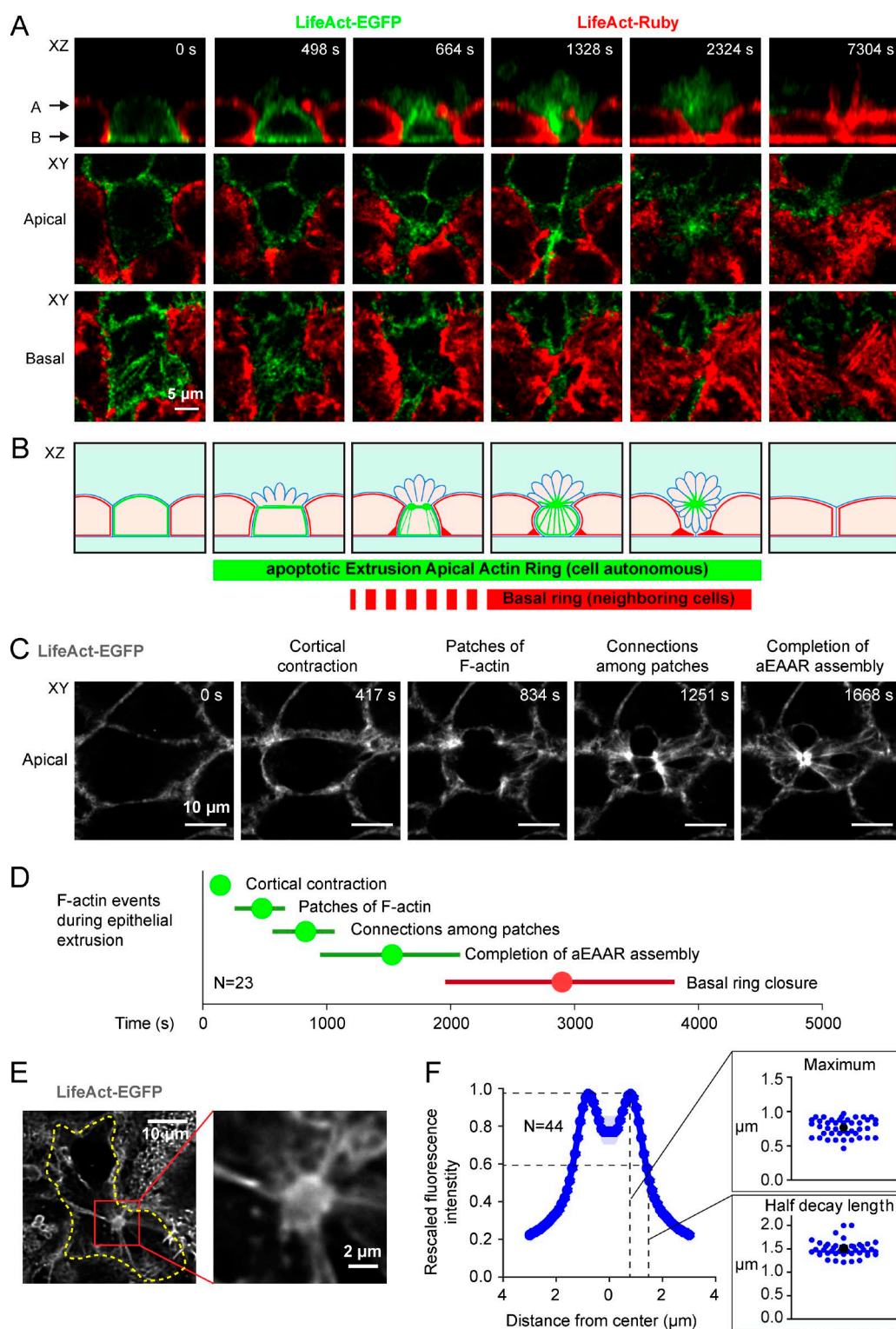
Figure 1.   **Assembly of one apical F-actin ring occurs within the extruding epithelial cell. (A)** The figure represents an epithelial MCF10A cell undergoing cell extrusion. The sequence of images are derived from *XY* and *XZ* optical sections of confluent epithelial cells MCF10A stably transduced with LifeAct-EGFP or LifeAct-Ruby and mixed at a 1:1 ratio. The extruding cell is stained with LifeAct-EGFP and shows the assembly of cell-autonomous aEAAR. **(B)** Cartoon representing the sequential events of epithelial extrusion according to our experimental observations. Blue, plasma membrane; green, F-actin of the extruding cell; red, F-actin of neighboring cells. **(C)** Grayscale image sequence of *XY* optical section of a representative aEAAR, showing four identifiable phases of its assembly: (1) cortical contraction, (2) formation of F-actin patches, (3) connection among patches, and (4) coalescence of patches in a unique ring-like structure. **(D)** Statistical analysis of time distribution of aEAAR assembly phases measured starting from the frame preceding cortical contraction. Extruding-cell autonomous events are represented in green, and events of neighboring cells in red. Discs represent the means, and horizontal bars SDs. **(E)** Left: Optical section of a cell with a fully assembled aEAAR detected by LifeAct-EGFP live staining (grayscale). Right, enlargement of the aEAAR. **(F)** F-actin density is measured as the fluorescence intensity of the aEAAR as a function of the distance from aEAAR center. The radial profile was calculated by taking the mean of the rescaled radial profile intensity of several aEAARs (*n* = 44). Insets: Distributions of distances from aEAAR center of maximum F-actin density and half decay length respectively. Blue dots, samples; black dot, mean.
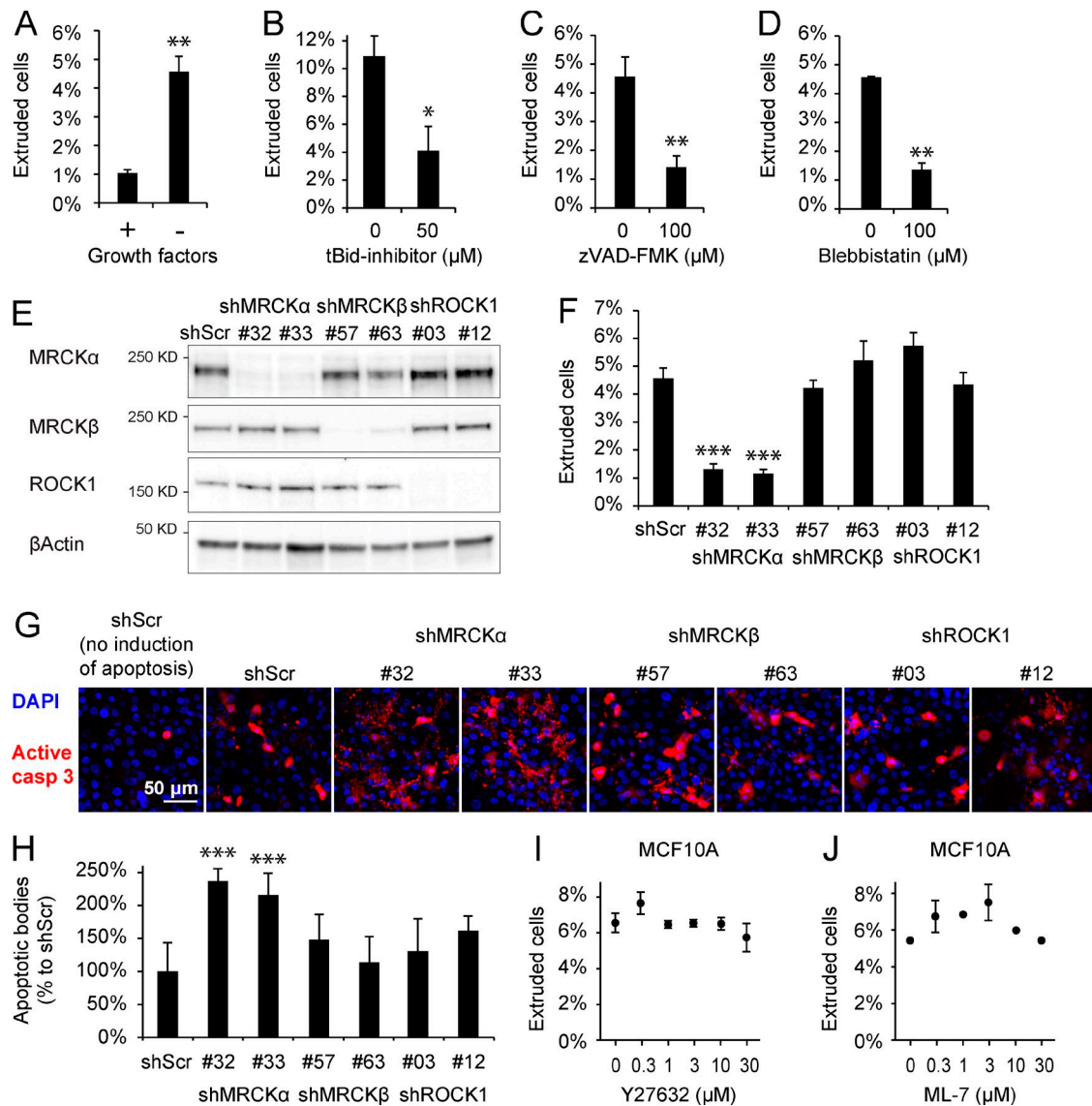
Figure 2. **Apoptotic epithelial extrusion relies on myosin contraction and MRCKα.** **(A)** Epithelial extrusion, measured by counting the number of cellular bodies released in the culture medium from confluent MCF10A epithelium, is significantly increased by removal of growth factors for 16 h. **(B)** Treatment with the tBid inhibitor (50 µM) caused a decrease in the number of extruded cells after growth factor deprivation. **(C)** The same effect was recapitulated by treatment with the caspase inhibitor zVAD-FMK (100 µM). **(D)** Inhibition of myosin contraction by blebbistatin (100 µM) hampered epithelial extrusion. **(E)** Efficiency of MRCKα, MRCKβ, and ROCK1 silencing shown by immunoblot. **(F)** The quantification of extrusion in cells stably silenced for MRCKα, MRCKβ, or ROCK1 shows that only MRCKα is able to significantly impair epithelial extrusion from confluent cells compared with control shRNA (shScr). In these experiments, error bars represent the SEM. **(G)** Evaluation of apoptotic cells present in confluent epithelial layer 16 h after apoptotic induction detected by anti–cleaved caspase 3 antibody (in red). Signal detected in the epithelial layer is the sum of not-yet-extruded cells and apoptotic bodies resulting from faulty extrusion. **(H)** Quantification of apoptotic bodies (size 1.6–12.5 µm^2) shows that extrusion-defective MRCKα silenced cells are forced to conclude apoptosis within the epithelial layer. **(I and J)** Extrusion assay in presence of different concentrations of Y27632 (I) and ML-7 (J) shows that apoptotic epithelial extrusion in MCF10A is independent of ROCK and MLCK. Error bars represent SEM (n = 3). *, P < 0.05; **, P < 0.01; ***, P < 0.001.

as shown by staining of active caspase 3 in MRCKα-silenced cells (Fig. 2 G). Notably, a consequence of a faulty extrusion process is that apoptotic cells are forced to terminate apoptosis within the epithelium, causing accumulation of apoptotic bodies. This phenotype was observed in MRCKα-silenced epithelial layers (Fig. 2 H). The independence of epithelial extrusion from ROCK1 was further confirmed by treatment with the ROCK inhibitor Y-27632, which showed lack of effect (Fig. 2 I).

In addition to the members of Rho kinase family, it has been described that MLC kinase (MLCK; Petrache et al., 2003) is activated by caspase-mediated cleavage during apoptosis.

To investigate the possible role of MLCK in actomyosin dynamics during epithelial extrusion, we exploited its inhibitor ML-7. However, treatment of MCF10A with ML-7 poorly affected apoptotic epithelial extrusion, excluding MLCK as a possible transducer in this cellular model (Fig. 2 J).

MRCKα kinase activity is regulated by caspase-mediated cleavage at aspartate 478

To understand how MRCKa is involved in apoptotic epithelial extrusion, we investigated whether MRCKα is cleaved during

apoptosis. Because of the high similarity of MRCKα and MRCKβ, we verified whether MRCKβ is cleaved as well.

We induced synchronous apoptosis by treating cells with the topoisomerase II inhibitor doxorubicin. Both MRCKα and MRCKβ are cleaved in shorter fragments during apoptosis in two different cell lines (Fig. S3, A and B). For both MRCKα and MRCKβ, the cleavage is mediated by caspases and prevented by treatment with the caspase inhibitor z-VAD-FMK (Fig. 3 A). However, although treatment with increasing concentrations of z-VAD-FMK revealed that MRCKβ is cleaved only in one site, we found that MRCKα is cleaved in two distinct sites showing two different sensitivities to inhibition (Fig. 3 A).

By measuring the electrophoretic path length, we estimated the localization of the caspase-cleavage sites in the two proteins: in MRCKα, the first cleavage site is localized at 464 ± 32 aa and the second one at 970 ± 48 aa, which corresponds to the MRCKβ cleavage site at 953 ± 82 aa (Fig. 3 B). In the region of the first MRCKα cleavage site, there is only one sequence showing a high score for caspase cleavage, which is absent in MRCKβ (Figs. 3 C, Fig. S3 C, and Fig. S4, A and B). In the second cleavage site of MRCKα, there are instead three putative cleavage sequences absent in MRCKβ. Unlike MRCKα, MRCKβ has only one putative cleavage sequence not present in MRCKα (Figs. S3 C and S4, C and D). All the caspase cleavage sites that we identified in MRCKα and MRCKβ have evolved in protein regions showing high probabilities for random coil secondary structures (Fig. S4). These regions have been described to host caspase cleavage sites more frequently than regions with defined secondary structure (Crawford et al., 2012).

To experimentally validate the identified cleavage sites, we performed a pull-down assay on a recombinant protein made by GFP and GST, intercalated with the putative cleavage sequence (Fig. 3 D). Our experiments demonstrate that MRCKα is efficiently cleaved at aspartates 478 and 971, whereas the cleavage is less efficient at aspartate 965 and nearly absent at aspartate 948 (Fig. 3 D and quantification in Fig. S3 D). The mutation of aspartates into alanines was used as a control to verify that cleavage is indeed mediated by caspases (Fig. 3 D).

To understand whether caspase-mediated cleavage of MRCKα results in regulation of kinase activity, we produced N-terminal GST-fused MRCKα. We cleaved it in vitro by active recombinant caspase 3 and measured the resulting kinase activity. We demonstrated that caspase 3 cleavage determines an increase of MRCKα kinase activity (Fig. 3 E). To prove that the cleavage at aspartate 478 is the cause of this increase in kinase activity, we produced and validated the uncleavable mutant MRCKα D478A (Fig. S3 E). This mutation is indeed sufficient to completely prevent the caspase-mediated increase of kinase activity (Fig. 3 E).

Caspase-cleaved MRCKα expression triggers iEAAR assembly and epithelial extrusion

The increase of MRCKα kinase activity is expected to determine a rearrangement of the actomyosin cytoskeleton through myosin phosphorylation. To investigate whether the MRCKα cleavage product, encompassing the kinase domain, is involved inEAAR assembly and epithelial extrusion, we transiently expressed mCherry-tagged MRCKα 1–478 in MCF10A cells. As soon as cells start to express mCherry-MRCKα 1–478, an actin-based structure that closely resembles the aEAAR is assembled at the apical side. We refer to this structure as "induced EAAR" (iEAAR) to distinguish it from aEAAR formed during apoptosis (Fig. 4 A and Video 4). The assembly of iEAAR is characterized by the same temporal sequence of events of aEAAR assembly (Fig. 4 B). To better understand the relationship between MRCKα 1–478 expression and iEAAR assembly, we quantified the amount of mCherry fluorescence as a function of time. We observed that the early phase of iEAAR assembly and the appearance of mCherry fluorescence are simultaneous events (Fig. 4 C).

The formation of iEAAR is specifically caused by the expression of the MRCKα 1–478 cleavage product, because neither the fluorescent tag alone nor full-length MRCKα is able to recapitulate this effect (Fig. 4, D and E). The expression of MRCKα 1–965 is more effective than the full-length protein to induce iEAAR assembly, while still being threefold less effective than MRCKα 1–478 (Fig. 4, D and E). In all cases, iEAAR induction depends on MRCKα kinase activity, as the mutant carrying a nonfunctional kinase domain does not have any effect on iEAAR assembly (Fig. 4, D and E). We never observed an incomplete iEAAR or other intermediate structures, suggesting that the iEAAR assembly is an on/off process that once activated cannot be interrupted (Fig. 4 E). The assembly of iEAAR was observed also in MDCK, HeLa, A431, and Caco2 cells transfected with MRCKα 1–478 (Fig. 5 A). The majority of MCF10A cells transfected with MRCKα 1–478 get extruded (Fig. 5, B and C; and Video 5), albeit with a variable latency compared with spontaneous apoptotic extrusion. This effect was abrogated when its kinase activity was abolished (Fig. 5 C). A similar effect was observed in MDCK cells (Fig. S5 A).

To exclude the possibility that MRCKα 1–478 indirectly induces iEAAR assembly through activation of programmed cell death, we treated MRCKα 1–478 transfected cells with the tBid inhibitor or zVAD-FMK. In all the cells analyzed, treatment with each of the two inhibitors had no effect on iEAAR assembly and cell extrusion (Fig. 5, D–F). Moreover, cells expressing MRCKα 1–478 were negative for active caspase 3 staining, further proving that cleaved MRCKα is directly able to induce iEAAR assembly and epithelial extrusion (Fig. 5 G).

ROCK1 role in iEAAR formation and epithelial extrusion

Although it is clear that, in MCF10A, apoptotic epithelial extrusion depends on MRCKα and not ROCK1, it would still be possible that caspase-mediated cleavage of ROCK1 plays a role as well. To investigate this possibility, we overexpressed YFP-ROCK1 1–1,113 in MCF10A cells, observing the induction of iEAAR assembly in the majority of cells (Fig. 6 A). Because iEAAR is driven by constitutive ROCK1 kinase activity, treatment with Y27632 effectively prevented iEAAR assembly (Fig. 6 B). The inhibitory effect of Y27632 was specific to iEAAR induced by YFP-ROCK1 1–1,113, as iEAAR assembly caused by mCherry-MRCKα 1–478 expression was not impaired (Fig. 6 C).

Therefore we took advantage of Y27632 specificity to investigate the role of ROCK1 in MDCK, Caco2, A431, and HeLa cells in which we recapitulated apoptotic extrusion. MDCK cells showed a basal rate of extrusion that is significantly reduced by the caspase inhibitor zVAD-FMK (Fig. 6 D). Caco2 and A431 are two epithelial cell lines that retain multiple epithelial features. Apoptotic epithelial extrusion can be specifically induced in these cell lines by doxorubicin treatment (Fig. S5 B) and reverted by caspase inhibition (Fig. 6 D). In addition, we observed that HeLa cells, despite having lost several
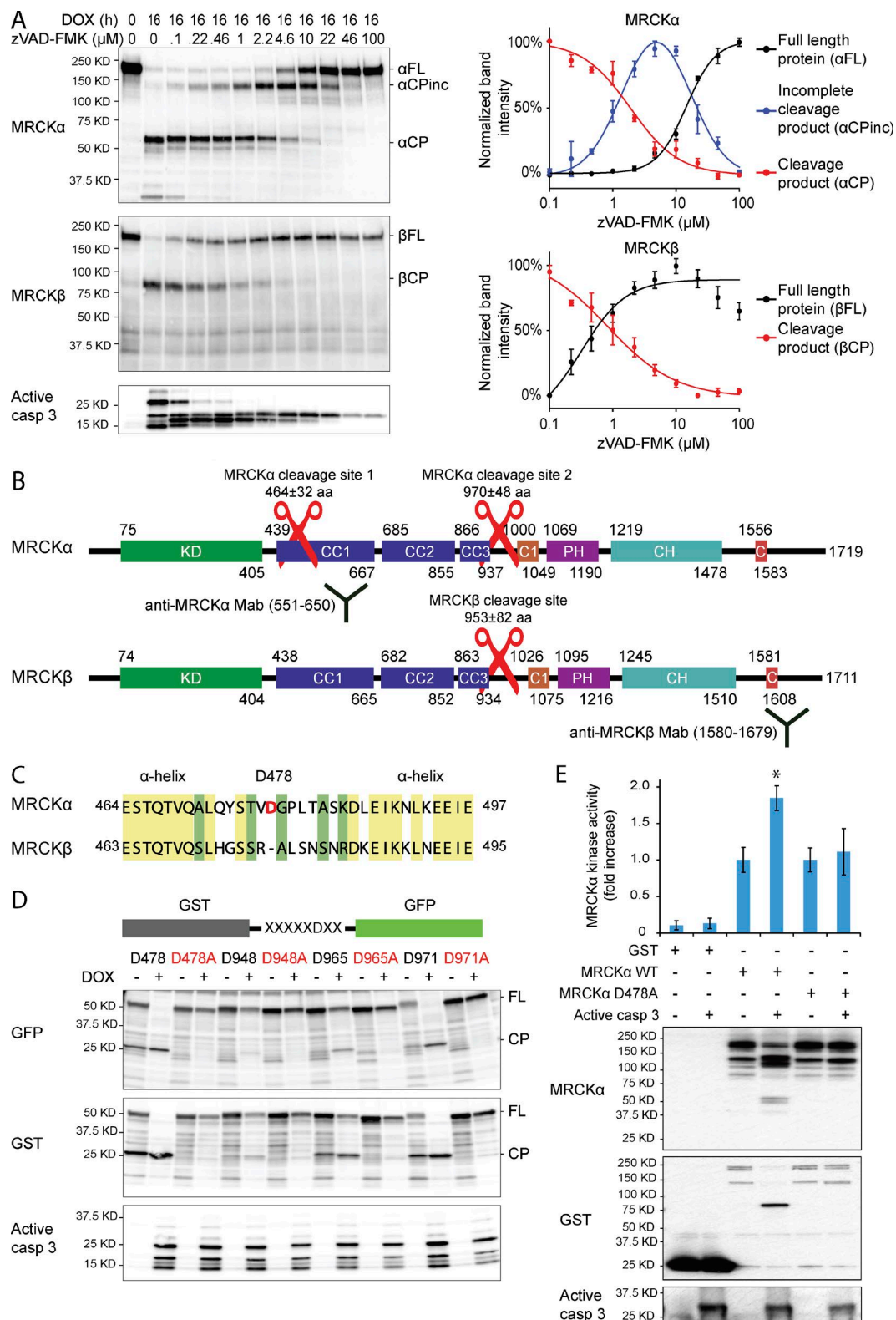
Figure 3. **Caspase-mediated cleavage of MRCKα at Asp 478 determines increase of its kinase activity. (A)** Caspase-mediated MRCKα and MRCKβ cleavage assay in HeLa cells treated with 10 μM doxorubicin for 16 h in combination with increasing concentrations of the caspase inhibitor zVAD-FMK shows that MRCKα is cleaved in two separates sites and MRCKβ in only one site. Left, representative experiment. Right, quantification and mean of six experiments. Error bars represent SD. **(B)** MRCKα and MRCKβ primary structures showing the different domains (kinase domain, KD; coiled coils domains, CC; protein kinase C conserved region 1, C1; pleckstrin homology-like, PH; citron homology, CH; CDC42/Rac interactive binding, C), the two antibody epitopes, and the estimation of cleavage regions as derived from electrophoretic path length of the cleavage products. **(C)** Sequence of MRCKα including Asp 478 compared with the homologue sequence in MRCKβ. Yellow background, conserved amino acids; green background, amino acids with similar features. **(D)** Cleavage screening of putative cleavage sequences in sites 1 and 2 of MRCKα. As negative controls, all the aspartates have been mutated

epithelial features during tumor progression, still maintain the ability to form a confluent layer in which it is possible to reproduce apoptotic extrusion. We induced this process in HeLa cells by treating a confluent layer with a low concentration of doxorubicin, inducing extrusion in <5% of cells (Fig. S5 B). We showed that this phenomenon depends, at least partially, on apoptosis (Fig. 6 D).

Although ROCK1 was dispensable for apoptotic epithelial extrusion in MDCK and A431 cells (Fig. 6 E), in addition to MCF10A (Fig. 2 I), its activity was required for HeLa and Caco2 cells (Fig. 6 E). We exploited this experimental approach to investigate also the role of MLCK in this panel of cell lines. We found that treatment with ML-7 was unable to prevent apoptotic epithelial extrusion in Caco2 and A431 cells, whereas it had a limited inhibitory effect of HeLa and MDCK cells (Fig. 6 F).

In summary we found that the cleaved form of both MRCKα and ROCK1 is able, when overexpressed, to induce iEAAR assembly. Furthermore, our findings suggest that epithelial extrusion is controlled either by MRCKα or ROCK1 depending on the cellular model.

iEAAR generates centripetal flow in F-actin bundles

F-actin in iEAAR is usually localized in mid-height position with multiple F-actin bundles oriented in different directions (Fig. 7, A and B). When observed in section with super-resolution STED microscopy, iEAAR looks like a ring with multiple F-actin bundles converging into the iEAAR with often nearly tangent angles (Fig. 7 C). Similarly to aEAAR, the iEAAR is characterized by a maximum of F-actin density 0.8979 ± 0.3186 µm from the iEAAR center whereas the half decay of F-actin is distributed at 1.7139 ± 0.3691 µm from the center (Fig. 7 D).

To get further insights on iEAAR dynamics, we performed photobleaching experiments on actin covalently bound to GFP (GFP-actin). We cotransfected cells with mCherry-MRCKα 1–478 and GFP-actin in subconfluent MCF10A cells, as we found that in this condition iEAAR associated bundles are more elongated and parallel to the bottom glass. In these transfected cells, we photobleached multiple segments of F-actin bundles and measured F-actin bundle velocity toward the iEAAR (Fig. 7, E and F; and Video 6). We measured the width of bleached segments and established that this does not change while flowing toward the ring, independently from the starting distance to the iEAAR (Fig. 7 G and Video 6). This observation indicates that no internal contraction is present within the bundles, i.e., each bundle behaves as an inextensible cable on the timescale under consideration (400 s). Typical F-actin flow in bundles is around 10 nm/s, with occasional bursts in velocity caused by detachment of bundles' terminals (Fig. 7 H and Video 6).

To understand whether F-actin flow speed in bundles was comparable with F-actin flow speed in aEAAR assembly occurring in spontaneous cell extrusion, we measured the speed by which the distinct F-actin patches coalesce to form the aEAAR. We found that F-actin patches coalesce together with a mean

speed of 10 nm/s, suggesting that different phases of assembly and dynamics of aEAAR and iEAAR share the same mean speed of F-actin flow (Fig. 7 I).

The presence of F-actin flow toward the iEAAR suggests that the iEAAR is a structure characterized by rapid turnover of actin. To investigate this hypothesis, we photobleached the entire iEAAR and observed a progressive fluorescence recovery (Fig. 7 J, Video 6, and Fig. 8 J, quantification). Surprisingly, we found that the iEAAR fluorescence recovery is a biphasic process, with an initial fast recovery followed by a slower recovery. Our data indicate that the fast initial fluorescence recovery is not determined by coplanar F-actin bundles flowing into the iEAAR, as recovery occurs before nonbleached segments of bundles reach the iEAAR (Video 6). On the contrary, coplanar F-actin flow toward the iEAAR is compatible with the slower recovery phase (Fig. 8 J). In addition, we found that the inner and the outer part of the iEAAR recover to very different extents, with a faster fluorescence recovery in the outer part and a much slower recovery in the inner part (Fig. S5 D).

Assembly and function of iEAAR rely on myosin activity

Because our results indicate that myosin activity is required for epithelial cell extrusion, we evaluated whether myosin activity is also involved in iEAAR assembly and extrusion induced by MRCKα 1–478. We indeed observed that iEAAR is highly enriched for phosphorylated myosin (Fig. 8, A and B). Super-resolved images showed that phosphorylated myosin is localized in patches in the external part of the F-actin ring and on bundles. Phosphorylated myosin was particularly enriched in bundles close to their interception with the iEAAR (Fig. 8 C). Moreover, we found that myosin activity is also functionally involved in iEAAR assembly and epithelial extrusion. Blebbistatin treatment is indeed able to prevent iEAAR assembly in a concentration-dependent manner (Fig. 8, D and E) and accumulation of phosphorylated myosin on iEAAR (Fig. 8 D). Importantly, blebbistatin also prevents extrusion of MRCKα 1–478 transfected cells (Fig. 8 F). In contrast, MLCK is not determinant for iEAAR formation (Fig. S5 C).

To demonstrate that F-actin flowing in bundles toward the iEAAR is dependent on myosin activity, we measured flow speed on bundles by cotransfecting subconfluent MCF10A cells with MRCKα 1–478 and GFP-actin, and then treating them with blebbistatin (Fig. 8 G and Video 7). As expected, myosin inhibition was able to completely abrogate F-actin flow in bundles toward the iEAAR (Fig. 8, G and I). Moreover, blebbistatin was able to completely abrogate GFP-actin fluorescence recovery within the iEAAR (Fig. 8, H and K; and Video 7), showing that accumulation of actin within the iEAAR is actually driven by myosin contractile activity. Accordingly, the fluorescence recovery in the outer part was reduced and overlapped with that of the inner part (Fig. S5 E). Altogether, these findings demonstrate that the iEAAR is a structure devoted to pull and accumulate actin bundles and that its mechanical activity is directly imputable to myosin contraction.

---

in alanines and compared in the same assay. Immunoblot with anti-GST and anti-GFP antibodies was used to detect the full-length (FL) proteins and their relative cleavage products (CPs). This experiment proves that the two most efficient cleavage sites of MRCKα are Asp 478 and Asp 971. **(E)** The increase of MRCKα kinase activity after caspase-mediated cleavage is shown by in vitro kinase assay. Pulled-down full-length MRCKα (wild type or D478A mutant) fused to GST were first incubated with recombinant-active caspase 3 then with an MRCKα-specific substrate. Error bars represent the SEM. Western blots show the efficiency of cleavage mediated by the recombinant-active caspase 3. *, P < 0.05; **, P < 0.01; ***, P < 0.001.
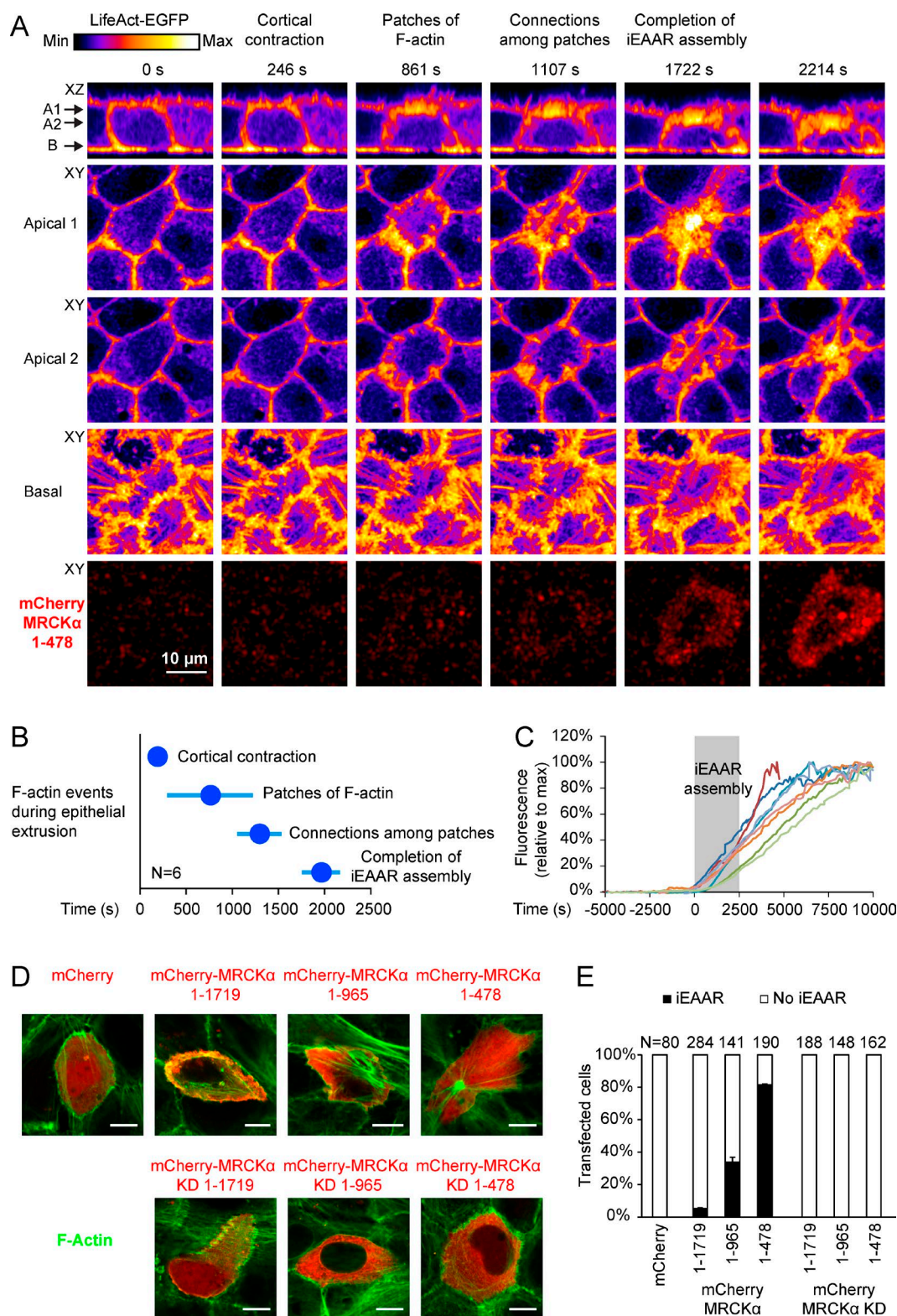
Figure 4. **MRCKα 1–478 cleavage product induces iEAAR assembly. (A)** The image sequence of live confocal microscopy shows a MCF10A cell, part of a confluent epithelium, that expresses mCherry-MRCKα 1–478 (red channel) and simultaneously assembles the iEAAR. Polymerized actin was represented with the fire color scale, to better visualize the different phases of iEAAR assembly. Because during the movie the iEAAR was moving downward, we show two *XY* apical sections. **(B)** Chronological analysis of the phases of iEAAR assembly in six cells expressing mCherry-MRCKα 1–478. Discs represent the means, and horizontal bars SDs. **(C)** Quantification of mCherry-MRCKα 1–478 fluorescence intensity as a function of the time. To compare different cells, raw fluorescence intensity data were normalized by setting the minimum fluorescence at 0% and the maximum at 100%. Each colored line represents a different cell. Gray box indicates the time required for iEAAR assembly based on the quantification in B, and time 0 was set at the frame preceding cortical contraction. **(D)** Confluent MCF10A cells were transfected with mCherry-fused full-length MRCKα (1–1,719), two shorter fragments (1–965 and 1–478), or their relative kinase dead (KD) mutants and evaluated for the formation of iEAAR detected by blebbistatin staining (green). Bars, 10 µm. **(E)** Frequency analysis of cells that, upon transfection with these constructs, assemble the iEAAR.
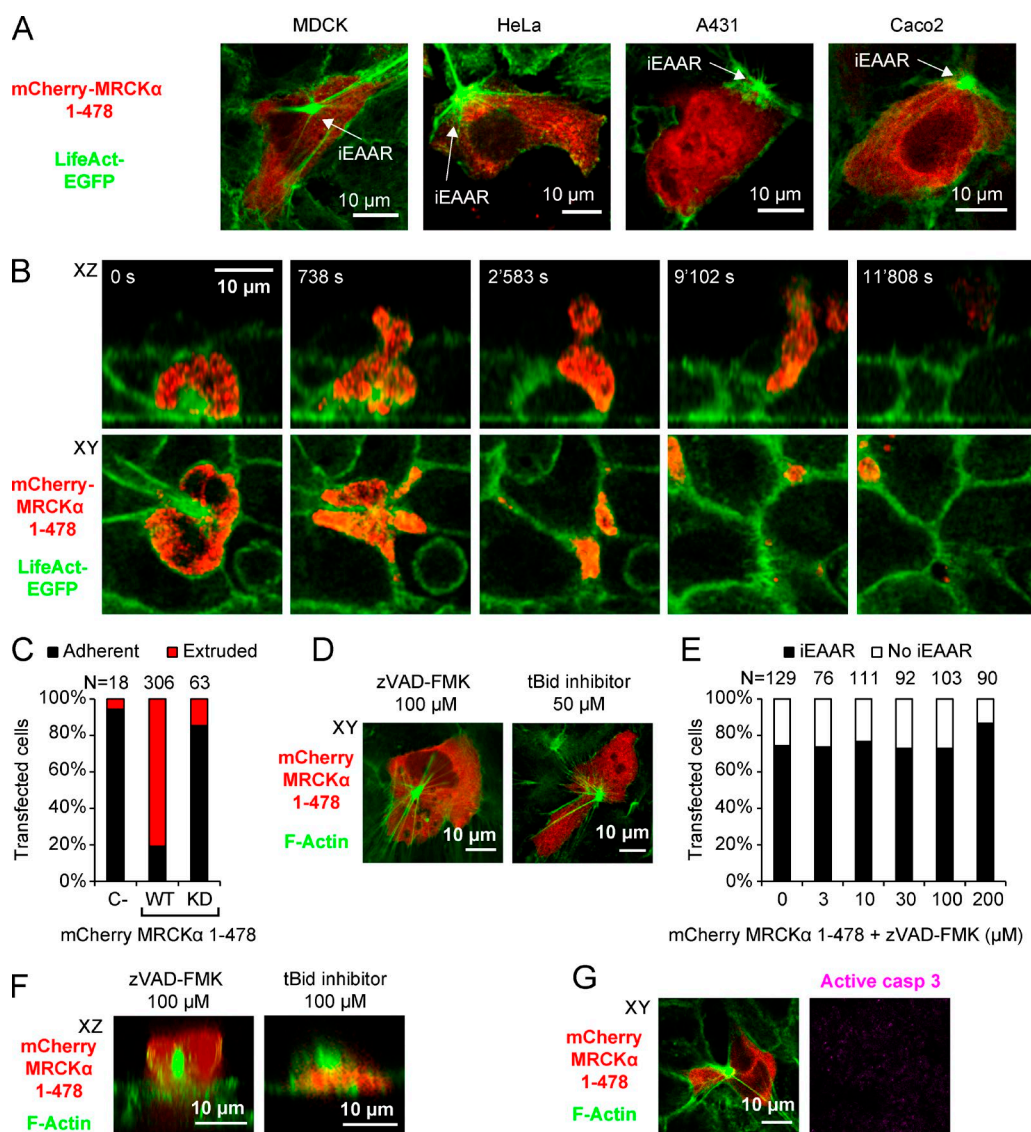
Figure 5. **MRCKα 1–478 cleavage product induces iEAAR assembly and epithelial extrusion. (A)** Transfection of mCherry-MRCKα 1–478 in MDCK, HeLa, A431, and Caco2 cells triggers iEAAR assembly. **(B)** Time-lapse sequence of a mCherry-MRCKα 1–478 expressing MCF10A cell undergoing the process of extrusion from a confluent epithelium. **(C)** Fate of MCF10A cells expressing mCherry alone, mCherry-MRCKα 1–478, or mCherry-MRCKα 1–478 KD. Cells were assigned to two categories: those that remained alive in the epithelium (Adherent) and those that were removed from the epithelium (Extruded). **(D)** MCF10A cells expressing mCherry-MRCKα 1–478 and show the presence of iEAAR despite the treatment with tBid inhibitor and the caspase inhibitor zVAD-FMK. **(E)** Analysis of the percentage of MCF10A cells transduced with mCherry-MRCKα 1–478 showing iEAAR in the presence of different concentrations of zVAD-FMK. **(F)** Treatment of MCF10A cells with tBid inhibitor or zVAD-FMK does not prevent epithelial extrusion induced in MCF10A by mCherry-MRCKα 1–478 transfection. **(G)** The expression of mCherry-MRCKα 1–478 in MCF10A induces the formation of iEAAR without the induction of apoptosis (negative for active caspase 3 staining).

Actin polymerization at the outmost bundles' terminals counteracts the action of the iEAAR

According to our observations, aEAAR formation and cell extrusion are consecutive events (Fig. 1, A and C). In the case of MRCKα 1–478 transduction, instead, cells remain adherent to the substrate for a variable period of time despite the presence of the iEAAR (typically 1–3 h) before the action of iEAAR itself causes cell collapse and detachment (Fig. 9 A and Video 8). Therefore, the life of a cell expressing MRCKα 1–478 can be divided in two phases: (1) a "tug-of-war" phase where the iEAAR/bundles system is well formed but the cell is still spread and adherent and (2) a "collapse" phase that shows the typical hallmarks of a blebbing apoptotic cell. During collapse, bundles shows high shortening rates that can reach tens or hundreds of nanometers per second (Fig. 9 B). In contrast, during the tug-of-war phase, the overall length of bundles is only slowly changing, with a mean shortening rate of less than 2 nm/s (Fig. 9 B, inset). This observation is in marked contrast to the relatively high flow rates observed in bundles (10–20 nm/s; Fig. 7, H and I).

This discrepancy can be reconciled by hypothesizing that at the outmost terminal of bundles, actin continuously polymerizes, thereby compensating for the actin flow in bundles and significantly reducing their shortening rate. We observed in detail the bundle terminals and found that shorter, downward bundles originate from RFP-vinculin focal adhesions, whereas longer bundles originate from RFP-vinculin negative cell edges (Fig. 9 C). Because it is well recognized that the adhesion sites
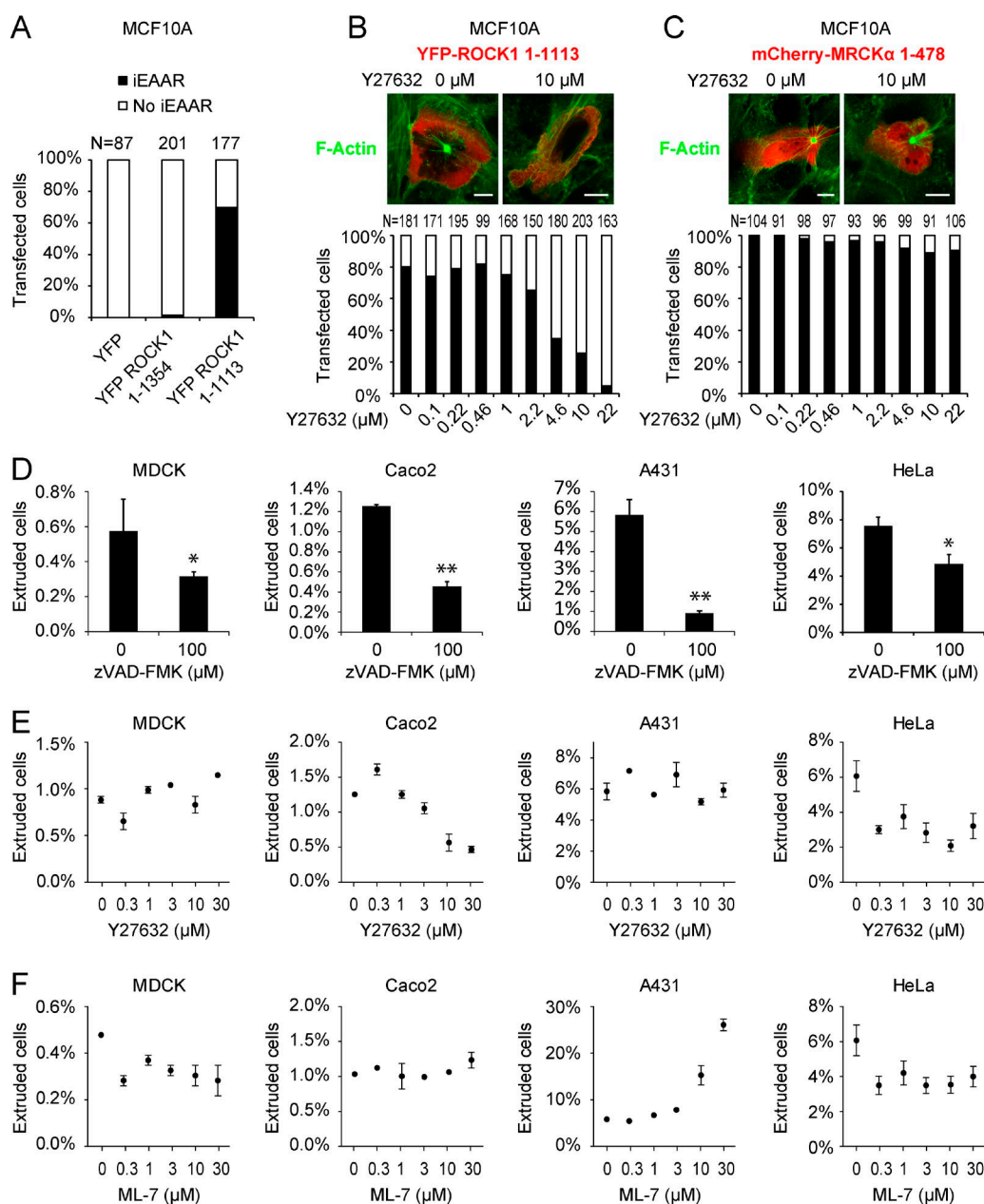
Figure 6. **ROCK1 role in iEAAR assembly and in the regulation of apoptotic epithelial extrusion. (A)** Percentage of MCF10A cells that show iEAAR formation after transfection with full-length YFP–tagged ROCK1 (YFP-ROCK1 1–1,354), with its apoptotic cleavage fragment (YFP-ROCK1 1–1,113) or YFP alone. Only YFP-ROCK1 1–1,113 is able to induce iEAAR assembly. **(B)** Treatment with Y27632 prevents iEAAR formation in MCF10A cells transduced with YFP-ROCK1 1–1,113. **(C)** Treatment with Y27632 fails to prevent iEAAR formation in MCF10A cells transfected with mCherry-MRCKα 1–478. Bars, 10 µm. **(D)** Apoptotic epithelial extrusion from confluent layer of HeLa, Caco2, MDCK, and A431 cells is prevented by the caspase inhibitor zVAD-FMK (n = 3). **(E)** The role of ROCK kinase activity in epithelial extrusion is shown in different cell lines by treating cells with different concentrations of Y27632 during the extrusion assay (n = 3). **(F)** The role of MLCK kinase activity in epithelial extrusion is shown the different cell lines by treating them with different concentrations of ML-7 during the extrusion assay (n = 3). *, P < 0.05; **, P < 0.01. Error bars represent SEM (n = 3).

host actin polymerizing activity (Hirata et al., 2008; Rao and Zaidel-Bar, 2016), we hypothesized the presence of this activity in iEAAR-associated bundles. To test this hypothesis, we photobleached the terminals of bundles in actin-GFP–transduced cells. We observed that indeed, polymerized unbleached actin originates within this bleached region through the addition of new actin to bundle terminals (Fig. 9 D and Video 9). The estimated speed of actin polymerization, based on the difference between actin flow speed and bundle shortening rate, is ~10 nm/s (Fig. 9 E).

To demonstrate that actin polymerization is required to compensate for actin flow speed during the tug-of-war phase, we decided to interfere with it by using two inhibitors with different mechanisms of action. Latrunculin A binds to G-actin, thereby preventing its polymerization at the plus ends of actin filaments. Cytochalasin D binds to the plus terminals of actin filaments, preventing both polymerization and depolymerization. As hypothesized, treatment with each of the two inhibitors caused a sudden increase of bundles' shortening, cell collapsing, and blebbing, simulating the phenotype of apoptotic
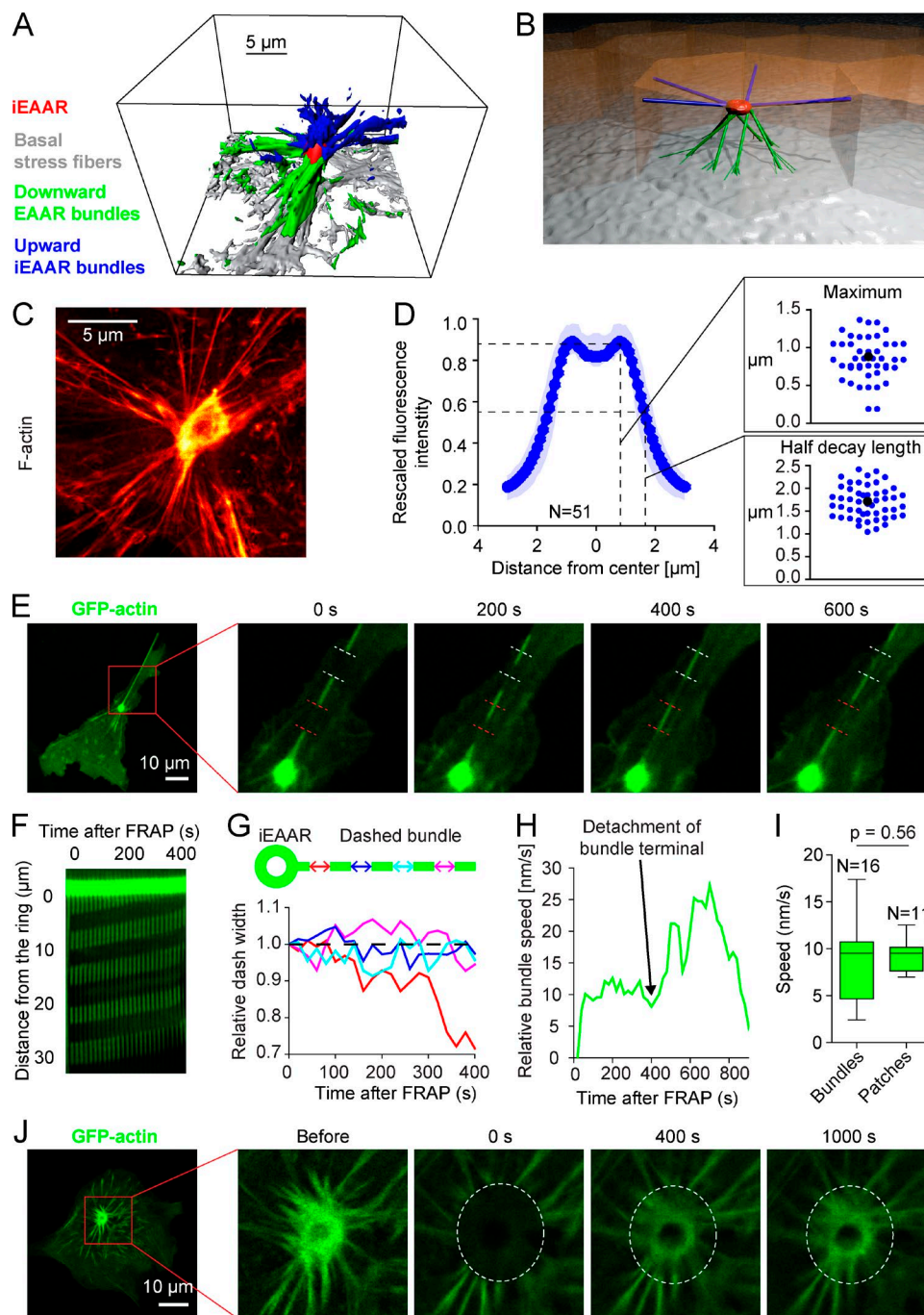
Figure 7. **iEAAR assembled after mCherry-MRCKα 1–478 transduction is a dynamic structure determining centripetal forces in multiple actin bundles. (A)** 3D reconstruction of F-actin cytoskeleton detected by phalloidin-488 staining in a MCF10A cell transfected with mCherry-MRCKα 1–478. The 3D reconstruction was performed starting from a multistack 3D STED acquisition. Surface rendering was obtained on the base of F-actin fluorescence intensity with Imaris software using the following parameters: smooth = true, surface grain size = 0.104666, diameter of largest sphere = 0.392498, manual threshold, and number of voxels above 10,000. In the representation we used the following color code: red, iEAAR; blue, upward bundles; green, downward bundles; gray, basal stress fibers. **(B)** Artistic 3D representation of an iEAAR (red), upward bundles (blue), and downward bundles (green). **(C)** STED nanoscopy image of an iEAAR assembled in a cell expressing mCherry-MRCKα 1–478. **(D)** F-Actin density was calculated as the mean fluorescence intensity as a function of the distance from iEAAR center. The radial profile was obtained by averaging intensity radial profile of several iEAARs (*n* = 51). Dark dotted line represents the mean values; light shades represent the area included between +SD and −SD. Insets: Distributions of distances from iEAAR center of maximum fluorescence intensity and half decay length, respectively. Blue dots, samples; black dot, mean. **(E)** Subconfluent MCF10A cells were cotransfected with GFP-actin and mCherry-MRCKα 1–478. Actin bundles were bleached in different regions, and movements of the bleached regions were monitored by time-lapse confocal microscopy. **(F)** Kymograph representation of the flow of bleached regions in the actin bundle shown in E. **(G)** Measurements of the length of the bleached regions as a function of time at different distances from iEAAR center (different colors) of the experiment in E. The segment represented by red line is shortening, because it is the closest one to the iEAAR and is absorbed into the iEAAR itself. **(H)** F-actin flow velocity in the dashed bundle of the experiment in E. **(I)** Comparison of distributions of actin flow velocities in iEAAR-associated bundles as obtained from bleaching experiments (Bundles) and velocity of F-actin patches coalescing during the assembly of aEAAR occurring in apoptotic epithelial extrusion (Patches). Box plots depict the median values (central line), 75th and 25th percentiles (upper and lower hinges), and maximum and minimum values (upper and lower whiskers). **(J)** Bleaching experiment of an iEAAR in a MCF10A cell cotransfected with GFP-actin and mCherry-MRCKα 1–478 showing recovery of fluorescence (quantification in Fig. 8 J).
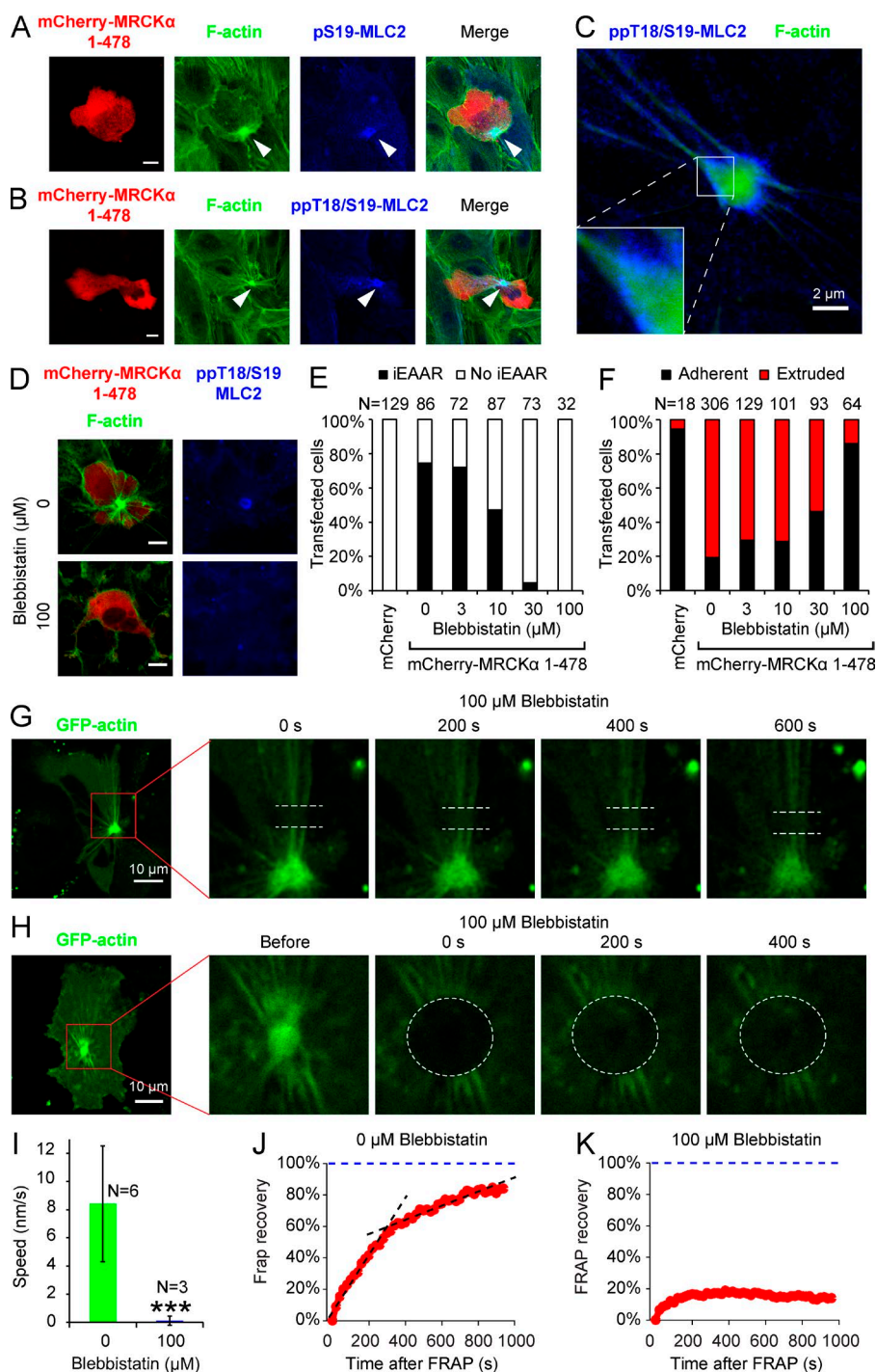
Figure 8. **Assembly of apical actin ring and epithelial extrusion rely on myosin activity. (A and B)** MCF10A cells transfected with mCherry-MRCKα 1–478 show, in correspondence with iEAAR, enrichment of phosphorylated regulatory subunit of myosin, detected with pS19-MLC2 (A) or pT18/S19 MLC2 (B) antibodies. **(C)** STED nanoscopy image of an iEAAR stained for F-actin and pT18/S19 MLC2. **(D)** Cells were transfected with mCherry-MRCKα 1–478 in the presence or absence of 100 µM blebbistatin and stained for F-actin (green) and pT18/S19 MLC2. Bars in A, B, and D, 10 µm. **(E and F)** Cells were transfected with mCherry alone (as negative control) or mCherry-MRCKα 1–478 in the presence of increasing concentrations of blebbistatin and evaluated for the frequency of iEAAR formation (E) and the frequency of extrusion (F). **(G and H)** Subconfluent MCF10A cells were cotransfected with GFP-actin and mCherry-MRCKα 1–478. Upon iEAAR assembly completion, cells were treated with 100 µM blebbistatin, and 10 min later, actin bundles (G) or the iEAAR itself (H) were bleached and monitored by time-lapse laser scanning confocal microscopy. **(I)** Actin bundle flow speed measured on the bleached region of cells treated or untreated with blebbistatin proves that myosin contraction is required for actin flow in bundles. Error bars represent the SD. **(J and K)** Fluorescence recovery of GFP-actin of iEAAR in absence (J) or presence (K) or of blebbistatin treatment. The fluorescence recovery curve of iEAAR shows a typical biphasic behavior that is abrogated by blebbistatin treatment. ***, P < 0.001.

cells and cells expressing MRCKα 1–478 in the collapse phase (Fig. 9, F and G; and Video 10). To demonstrate that the increase of iEAAR bundles' shortening rate and cell collapse is caused by myosin contraction, we simultaneously treated cells with cytochalasin D and blebbistatin. The presence of blebbistatin was sufficient to block iEAAR bundles' shortening and cell collapse (Fig. 9, F and G; and Video 10). This experiment demonstrates that actomyosin machinery in the iEAAR is responsible for the increase of bundle shortening rate caused by the inhibition of actin polymerization.

In summary, these observations demonstrate that (1) cell collapse can be induced in the tug-of-war phase by the block of

actin polymerization at the bundles' terminal; and (2) myosin activity alone is not sufficient to drive cell collapse and cell detachment, and therefore must be coupled with a down-modulation of actin-polymerizing activity (Fig. 10 A).

Discussion

Here we describe the characterization of a ring-shaped actomyosin structure (termed EAAR) orchestrating the morphological events of apoptotic cells during epithelial extrusion. These events are triggered by caspase-mediated cleavage of
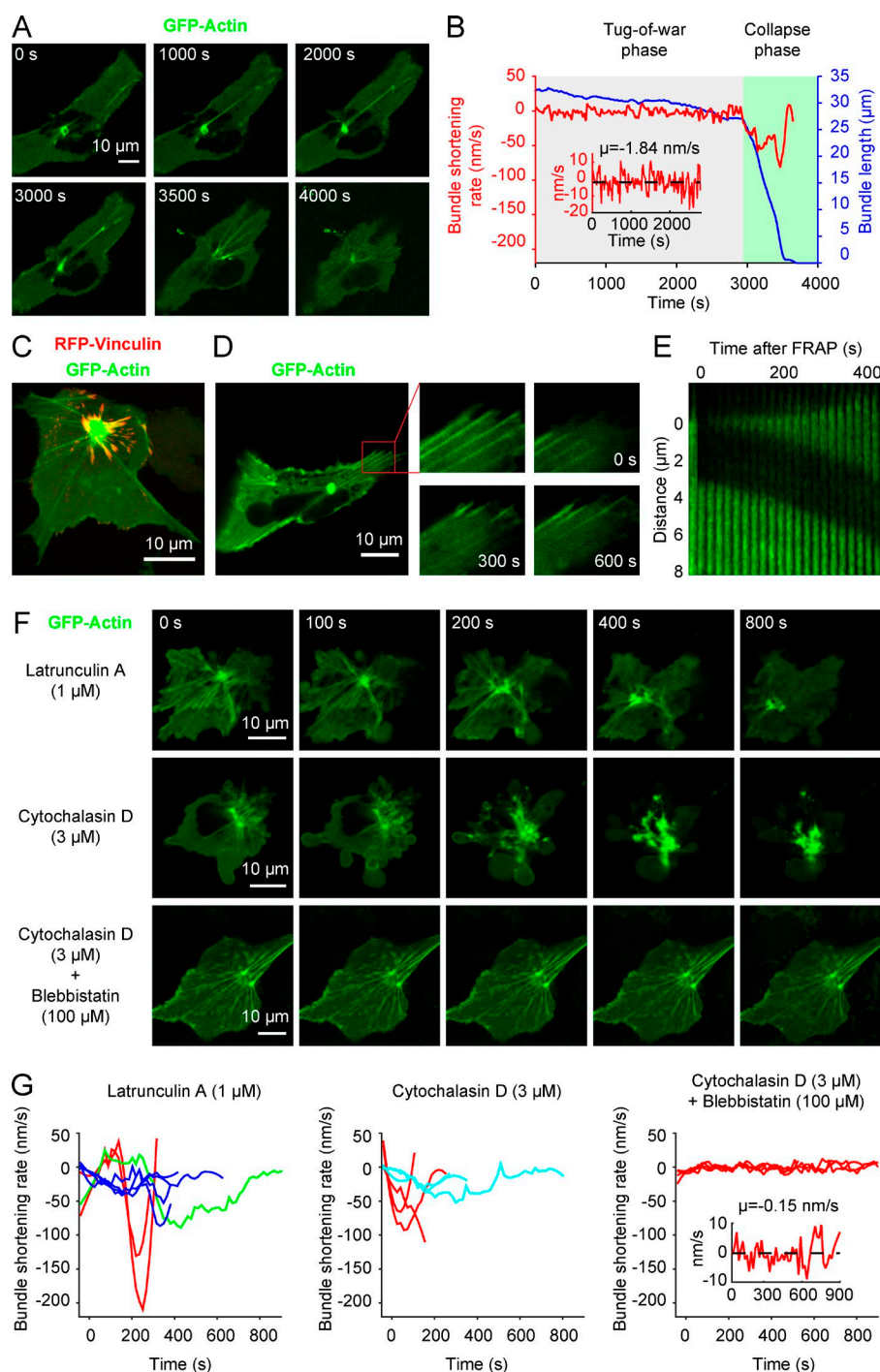
Figure 9. **Actin polymerization at the outermost bundle terminals balances centripetal forces generated by the iEAAR.** (A) A cell coexpressing mCherry-MRCKα 1–478 and GFP-actin shows a long phase where shape, iEAAR, and associated bundles are maintained with minimal morphological variation followed by a shorter phase of sudden cell collapse and synchronous shortening of bundles. (B) Quantification of the length and shortening rate of one bundle from time-lapse experiment in A. Two distinct phases are identifiable: (1) a tug-of-war phase characterized by slow bundle shortening and (2) a collapse phase where the bundle is subjected to a rapid shortening until its complete adsorption within the iEAAR. Inset, enlargement of the shortening rate in the tug-of-war phase showing a slow and noisy reduction of the length of the bundle. (C) A cell cotransfected with GFP-actin, GST-MRCKα 1–478, and vinculin-RFP showing an iEAAR ring with shorter, downward bundles originating from cell–matrix adhesions and long bundles originating from cell edges, likely the site of cell–cell adhesions. (D) A cell cotransfected with GFP-actin and mCherry-MRCKα 1–478 was bleached at the bundles' terminals and monitored by time-lapse confocal microscopy. (E) Kymograph showing actin polymerization of a photobleached bundle terminal. (F) Subconfluent MCF10A cells were cotransfected with GFP-actin and mCherry-MRCKα 1–478 then treated with 1 µM latrunculin A, 3 µM cytochalasin D, or cotreated with 100 µM blebbistatin and 3 µM cytochalasin D. Blockage of actin polymerization caused by latrunculin A and cytochalasin D causes rapid cell collapse, which is prevented by blebbistatin treatment. (G) Shortening rate of bundles in GFP-actin and mCherry-MRCKα 1–478 expressing cells treated with 1 µM latrunculin A, 3 µM cytochalasin D, or cotreated with 100 µM blebbistatin and 3 µM cytochalasin D. Each color encodes for a different cell, whereas curves of the same color represent different bundles in the same cell. Inset, enlargement of the shortening rate in cells cotreated with latrunculin A and cytochalasin D.

MRCKα that is able to potently increase the kinase activity on the regulatory subunit of nonmuscular myosin (Fig. 10 B). The consequent massive and ubiquitous phosphorylation of myosin complexes causes rapid cell contraction, assembly of the EAAR, and epithelial cell extrusion (Fig. 10 C).

The role of MRCKα in reorganization of actomyosin structures is of particular relevance in the wider context of cytoskeletal rearrangements occurring during apoptosis. Indeed, during this process, cytoskeletal proteins might be exploited in a nonconventional function by being activated or conversely inactivated. The latter is the case of intermediate filament components (e.g., desmin, vimentin, lamin), whose assembly is prevented by caspase-mediated proteolytic cleavage (Rao et al.,

1996; Byun et al., 2001; Chen et al., 2003). Microtubules, after initial disassembly, are coopted to form the apoptotic microtubule network (Oropesa-Ávila et al., 2013).

Similarly, it was proposed that actin cytoskeleton is degraded by caspases and disassembled (Brown et al., 1997; Mashima et al., 1999). However, this occurrence is in sharp contrast with our observations, which demonstrate that the actin cytoskeleton is fully able to organize itself in high-order structures during apoptosis. Nonetheless, many other observations identify the actomyosin cytoskeleton as the main force-generating structure in apoptotic cells (Desouza et al., 2012). Indeed, most of the peculiar events of apoptosis rely on the actomyosin cytoskeleton, including cell body
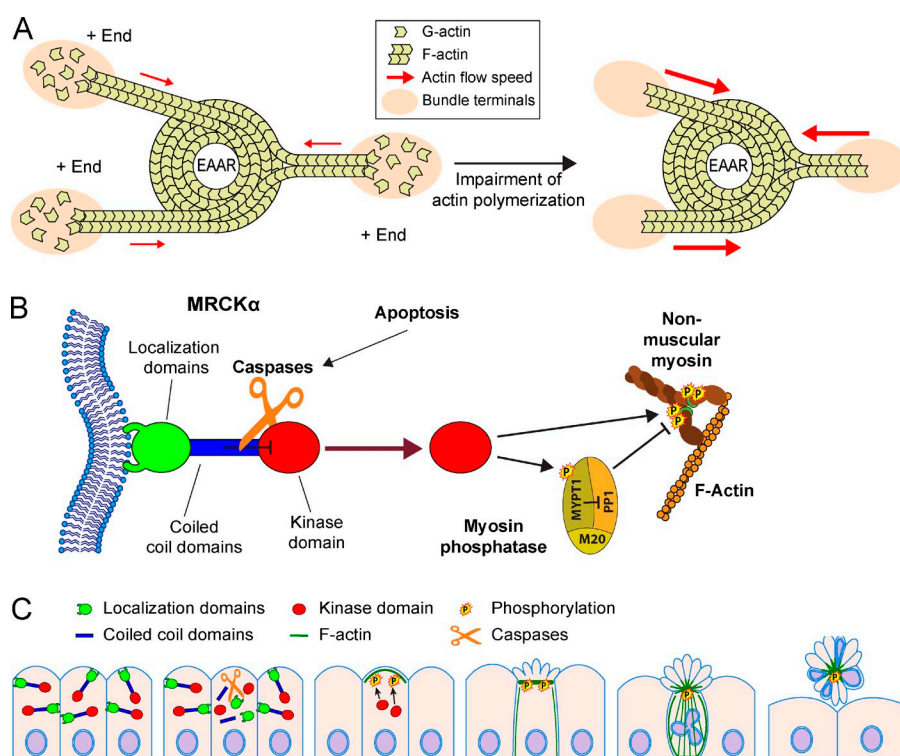
Figure 10. **MRCKα controls EAAR assembly and epithelial extrusion. (A)** Cartoon showing the role of actin polymerization in EAAR mechanics. Actin is continuously assembled at the outermost bundle terminals (+ ends) coinciding with adhesion sites. The fast polymerizing activity occurring at the + ends is able to compensate for the actin flow generated by the centripetal pulling activity of EAAR, reducing the overall tension (red arrows) applied on bundles. Whenever actin polymerization activity is blocked, the uncompensated actin flow in bundles causes a rapid increase in bundle tension (red arrows) and a sudden increment of shortening rates of bundles, detachment of adhesions, and cell collapse. This model suggests that an efficient process of extrusion requires the coupling of myosin activity in the EAAR and down-modulation of actin polymerization at the bundles' terminals. **(B)** MRCKα is a protein constituted by multiple domains that can be subclassified in three regions according to their functions: an N-terminal kinase domain (red), a central region composed of three coiled-coil domains (where CC2 and CC3 have inhibitory activity on the kinase domain; blue), and a C-terminal region including different domains deputed to binding to plasma membrane (green). Upon apoptosis activation, caspases cleave MRCKα in three parts corresponding to these three functional regions. The kinase domain is therefore relieved from the inhibitory activity exerted by CC2 and CC3 domains and is uncaged from the localization domains, acquiring solubility in the cytoplasm. The kinase domain, now free to reach and phosphorylate the regulatory small subunit of the nonmuscular myosin, promotes a massive contractile activity. This mechanism is further enforced by the phosphorylation of MYPT1 subunit of myosin phosphatase, preventing its inhibitory activity on myosin, and by the concomitant activation of other myosin kinases, such as ROCK1 and MLCK. **(C)** Caspase-mediated activation of MRCKα plays a crucial role during epithelial extrusion, by causing cortical contraction and EAAR assembly through the phosphorylation of the regulatory subunit of myosin. By generating centripetal forces, the EAAR causes shortening of actin bundles, collapse of cell body, and an upward movement of apoptotic cells toward the apical side of the epithelial layer. This sequence of events is required during epithelial extrusion, which is finally completed by basal ring constriction determined by the concerted action of neighboring cells.

shrinkage (Núñez et al., 2010), membrane blebbing (Coleman et al., 2001), nuclear disintegration (Croft et al., 2005), apoptotic body formation (Coleman et al., 2001), and epithelial cell extrusion (Rosenblatt et al., 2001).

Actomyosin machinery has been shown to be regulated in a nonconventional manner during apoptosis. Caspase-mediated cleavage irreversibly activates both ROCK1 (Coleman et al., 2001; Sebbagh et al., 2001) and MLCK (Petrache et al., 2003), causing constitutive phosphorylation of MLC2. Such a mechanism of activation is shared by MRCKα, as we demonstrated, and likely underlies the need for a rapid and strong burst of myosin phosphorylation.

The main consequence of MLC2 phosphorylation burst promoted by MRCKα cleavage is the assembly of EAAR. This unique higher-order actin-based structure is constituted of a ring-shaped central structure with multiple F-actin bundles converging into it. Although a ring-like dense structure has already been reported during epithelial apoptosis, it occurs basally and is formed by the cooperation of apoptotic and neighboring cells (Rosenblatt et al., 2001). EAAR is instead functionally and spatially distinct from the basal extrusion ring according to multiple factors: (a) it is cell autonomous, (b) it is clearly separated from cortical actin, (c) it has a fixed size, and (4) it is associated with multiple F-actin bundles converging into the structure. Our findings therefore agree with a previous study showing that epithelial extrusion is a biphasic process, where basal ring constriction is invariably preceded by the formation of an apical dense actin structure (Kuipers et al., 2014).

Apical constriction is an important morphogenetic event even in contexts other than apoptosis, such as during development. The MRCKα homologous protein in *Caenorhabditis elegans*, named MRCK-1, has been described to regulate apical constriction during gastrulation (Marston et al., 2016). Apical constriction is also crucial in invagination processes, such as gastrulation and neural tube formation, during vertebrate development (Martin and Goldstein, 2014). At least two main types of apical constriction have been identified so far: contraction of a belt of F-actin and myosin at the apical circumference underlying adherens junctions and the contraction of a "medio-apical" actomyosin structure at the middle of the apical domain (Martin and Goldstein, 2014). Although the EAAR shows poor resemblance to actomyosin cytoskeleton structures involved in apical constriction, it shares with them localization and common regulators (MRCK and ROCK), suggesting a possible scenario in which the EAAR would derive from the basic mechanisms of apical constriction.

Overall, our observations on actomyosin contractility during epithelial extrusion support a cell-autonomous role of the apoptotic cell in this process. Indeed the EAAR acts as a centripetal spool pulling multiple F-actin bundles, therefore generating tension on adhesions and determining cellular body squeezing. The action of EAAR allows the cellular body to be pulled upward and finally to be extruded (Fig. 10 C). Moreover, the observation that the expression of a MRCKα cleavage fragment is alone sufficient to determine EAAR assembly and extrusion is proof that the EAAR is sufficient to generate the

forces required for cell extrusion without the whole apoptotic program being activated.

Proper execution of epithelial extrusion also requires the closure of the basal actomyosin ring. This event is the consequence of the apoptotic cell communicating its status to its neighbors by biochemical cues, such as sphingosine 1 phosphate (Gu et al., 2011). However, the observation that MRCKα cleavage fragment is alone sufficient to trigger an extrusion program raises the question whether the MRCKα downstream signal is transduced to surrounding cells. One intriguing possibility is that the extruding cell is able to communicate mechanic cues to neighboring cells through cell–cell adhesion (Lubkov and Bar-Sagi, 2014; Michael et al., 2016).

In summary, by describing a novel role of MRCKα during apoptosis, we cast light on the complex actomyosin cytoskeleton dynamics in the process of epithelial cell extrusion and, likely, in the homeostatic maintenance of tissues in multicellular organisms.

Materials and methods

Cell lines
MCF10A (CRL-10317), 293T (CRL-11268), MDCK (CCL-34), Caco2 (HTB-37), A431 (CRL-1555), and HeLa (CCL-2) cell lines were obtained from ATCC. All experiments were performed on cell lines that had been passaged for <3 mo after thawing. 293T, A431, and HeLa cells were cultured in DMEM, Caco2 in RPMI, and MDCK in Eagle's minimum essential medium (Sigma-Aldrich). Culture media were supplemented with 10% FBS (Gibco), 200 U/ml penicillin, and 200 µg/ml streptomycin (Sigma-Aldrich). MCF10A cells were cultured as described previously (Debnath et al., 2003). Transient gene expression in MCF10A cells was performed by using X-tremeGENE Transfection Reagents (Roche) and in HeLa cells by using Lipofectamine (Thermo Fisher Scientific).

Antibodies and reagents
Rabbit anti-pS19MLC2, rabbit anti-pT18/S19 MLC2, and rabbit cleaved caspase 3 (Asp175) antibodies were purchased from Cell Signaling Technology. Mouse monoclonal anti-MRCKα antibody and mouse anti-GST (B-14) were from Santa Cruz Biotechnology. Mouse anti-CDC42BPB clone 2F4 (anti-MRCKβ) was from Sigma-Aldrich. Rabbit anti-GFP was from Thermo Fisher Scientific. Phalloidin-Atto 488, Phalloidin-Atto 594, blebbistatin, doxorubicin hydrochloride, ML-7 (MLCK inhibitor), Y-27632, tBid inhibitor BI-6C9, cytochalasin D, and latrunculin A were purchased from Sigma-Aldrich. zVAD-FMK was purchased from Merck-Millipore.

Plasmids
pEGFP-actin was purchased from Clontech. Full-length MRCKα WT and MRCKβ kinase domain (KD) were provided by the T. Leung laboratory, Institute of Molecular and Cell Biology, A-STAR, Singapore (Leung et al., 1998; Tan et al., 2001). Full-length MRCKα and all the derived constructs (MRCKα 1–478, MRCKα 1–478 KD, MRCKα 1–965, MRCKα 1–965 KD, and MRCKα D478A) were cloned into pDONR/zeo using Gateway BP Clonase as previously described (Gagliardi et al., 2014). ROCK1 and ROCK2 constructs were cloned from full-length coding sequences provided by J. Herskowitz (University of Alabama at Birmingham, Birmingham, AL; Swanger et al., 2016). From pDONR/zeo, the constructs were transferred through Gateway LR Clonase in the following destination vectors: pcDNADEST47 (C-Term GFP),

in pcDNA-DEST53 (N-Term GFP), in pcDNA-C-mCherry (C-term mCherry), and in pDEST27 (GST-N-Term Tag), all from Invitrogen.

Dual-tagged (GST and GFP) constructs for screening of caspase-cleavage sequences were prepared as follows: GFP was amplified by PCR using primer couples for the BP Gateway reaction, where each forward primer includes one sequence coding for the polypeptides to be tested for caspase-cleavage (eight amino acids, six preceding the putative cleavage site and two after). Once obtained by cloning in pDONR/zeo, constructs were moved in pDEST27 (GST-N-Term Tag).

Gene expression analysis
Gene expression analysis was performed by quantitative real-time PCR. Total cellular RNA was isolated using the SV Total RNA Isolation kit (Promega). To quantify the expression levels of the genes of interest, equal amounts of cDNA were synthesized using the Moloney murine leukemia reverse transcription (Promega) and mixed with SsoFast Eva-Green Supermix (Bio-Rad) and 300 µM of each of the respective forward and reverse primers. Quantitative real-time PCR was done on a MyiQ thermal cycler (Bio-Rad). Each target gene expression was evaluated using a relative quantification approach, with GAPDH as an internal reference. The following primer couples were purchased from Bio-Rad: MRCKα (qHsaCID0009361), MRCKβ (qHsaCID0021825), MRCKγ (qHsaCID0036788), ROCK1 (qHsaCID0017481), ROCK2 (qHsaCID0018000), CIT (qHsaCED0043968), DMPK (qHsaCID0014430), and GAPDH (qHsaCED0038674). PCR cycling conditions were as follows: 30 s at 95°C, 5 s at 95°C, plus 30 s at 58°C (40 cycles).

In silico screening for caspase cleavage
MRCKα (NP_003598.2), MRCKβ (NP_006026.3), MRCKγ (NP_059995.2), ROCK1 (NP_005397.1), ROCK2 (NP_004841.2), CIT (NP_001193928.1), and DMPK (NP_001075032.1) protein sequences were analyzed as follows. Caspase cleavage probability was calculated through ScreenCap3 web server (Fu et al., 2014). Only sites showing caspase cleavage probability >0.7, with an estimated precision of 0.898, were considered. The obtained cleavage sites were further filtered for those sites showing mean random loop probability from P4 to P4′ > 0.5, calculated with the GOR IV method (Garnier et al., 1996).

Lentivirus production
For stable silencing of MRCKα, MRCKβ, and ROCK1, two pLKO.1 lentiviral vectors carrying targeting shRNA were used for each gene. For MRCKα, we used shMRCKα#32 (TRCN0000001332; Sigma-Aldrich) and shMRCKα#33 (TRCN0000001333). For MRCKβ, we used shMRCKβ#57 (TRCN0000195057) and shMRCKβ#63 (TRCN0000199663). For ROCK1, we used shROCK1#03 (TRCN0000194903) and shROCK1#12 (TRCN0000121312). A vector leading the expression of a scrambled nontargeting shRNA, called shScr, Addgene plasmid 1864 (Sarbassov et al., 2005), was used as a negative control. pLenti.PGK.LifeAct-GFP.W and pLenti.PGK.LifeAct-Ruby.W were gifts from R. Lansford (The Saban Research Institute, Los Angeles, CA; plasmids # 51010 and # 51009; Addgene).

Lentiviruses were produced by calcium phosphate transfection of lentiviral plasmids together with packaging (pCMVdR8.74) and envelope (pMD2.G-VSVG) plasmids in 293T cells as previously described (Gagliardi et al., 2012, 2015). Supernatant was harvested 24 and 48 h after transfection, filtered with 0.45-µm filters, precipitated (19,000 g for 2 h at 20°C), and suspended in PBS at a higher concentration. The multiplicity of infection was determined by infecting HeLa cells in presence of 8 µg/ml polybrene. The quantification of GFP-positive cells was performed by flow cytometry and that of puromycin-positive cells by puromycin selection and crystal violet staining.

Induction of epithelial extrusion

MCF10A, HeLa, MDCK, Caco2, and A431 cells were cultured in adhesion until stable confluence was reached (in the case of MCF10A cells this stable confluence state is maintained for more than 30 d) in complete medium (renewed every 2–3 d). To induce random apoptosis in a low percentage of cells, confluent epithelia of MCF10A and MDCK cells were maintained for 16 h in medium deprived of growth factors and serum: DMEM/F12 complemented with only 200 U/ml penicillin and 200 µg/ml streptomycin (Sigma-Aldrich). To induce apoptotic epithelial extrusion in HeLa, Caco2, and A431 cells, confluent epithelia were treated with different concentrations of doxorubicin (1, 100, and 3 µM, respectively).

Cell supernatant, containing the extruded cells, was collected, centrifuged, and suspended in a small volume of PBS (1:10 of the original volume). Density of extruded cells was measured by Countess automated cell counter (Thermo Fisher Scientific) using the following parameters: sensitivity 8, min size 5 µm, max size 60 µm, and circularity 80. The percentage of extruded cells was calculated according to the following formula: (extruded cell density × resuspension volume)/total number of cells in the well.

To visualize nonextruded cells, adherent cells were fixed with 3.7% PFA after 16 h of treatment with starving medium and accurate washing with PBS to remove all the extruded cells. Then, fixed epithelium was permeabilized with PBS 0.1% Triton X-100 (Sigma-Aldrich) and immunostained for anti–active caspase 3. Optical sections of the stained samples were acquired by means of confocal microscopy, and then the images were segmented and subjected to particle analysis with ImageJ software. The number of apoptotic bodies was measured by counting particles with size between 1.6 and 12.5 µm^2. These experiments were performed at least in triplicate.

Induction of MRCKα/β caspase-mediated cleavage

To observe the caspase-mediated cleavage of MRCKα/β, MCF10A and HeLa cells were treated with 10 and 25 µM doxorubicin, respectively, for 16 h. The treatment was used to induce simultaneous and widespread induction of apoptosis. All cells (both adherent and detached) were collected in a tube, washed twice with PBS, and lysed in Laemmli buffer. To investigate the caspase-mediated cleavage of exogenously expressed proteins, HeLa cells were transfected with Lipofectamine. 24 h after transfection, cells were subjected to doxorubicin treatment and lysis in Laemmli buffer.

In vitro caspase cleavage and kinase assay

pDEST27 empty vector, pDEST27-MRCKαWT, or pDEST27-MRCKαD478A plasmids were transfected in 293T cells with calcium phosphate (Promega). After 24 h, cell lysates were extracted using ice-cold lysis buffer (25 mM Hepes, 300 mM NaCl$_2$, 1 mM PMSF, 1.5 mM MgCl$_2$, 0.5% Triton X-100, 20 mM Na-β-glycerophosphate, 1 mM Na$_3$VO$_4$, 0.2 mM EDTA, and 1:1,000 protease inhibitor cocktail; Sigma-Aldrich). GST-tagged proteins were pulled down by means of glutathione Sepharose 4B beads (GE Healthcare). The isolated proteins were then eluted from Sepharose beads using reducing buffer (10 mM L-glutathione reduced and 50 mM Tris-HCl, pH 8.0) and subjected to caspase cleavage.

Recombinant active caspase 3 was dissolved in resuspending buffer (25 mM Hepes, 300 mM NaCl$_2$, and 10% glycerol), diluted in cleavage buffer (25 mM Hepes, 100 mM NaCl$_2$, 1 mM EDTA, 10% glycerol, 10 mM DTT, and 0.1% CHAPS) and added to the GST-fused eluted samples. Caspase cleavage reaction was performed at 30°C.

After caspase-mediated proteolytic cleavage, samples were used for kinase assay to monitor MRCKα kinase activity by means of ROCK Activity Assays (STA-416-5; Cell Biolabs). This assay is based on a solid-phase ELISA that uses a plate precoated with a specific synthetic peptide derived from myosin phosphatase target subunit 1 (MYPT1), which contains Thr696 residue, a common substrate for both ROCK and MRCK. For kinase assay, samples were diluted in Kinase Assay Dilution Buffer. The kinase reaction was then started by the addition of 2 mM ATP (which was previously diluted in Kinase assay dilution buffer and 10 mM DTT) and maintained at 30°C for 1 h. After completion of the kinase reaction, samples were recovered and analyzed by immunoblot. The phosphorylated substrate was detected with an anti–phospho-MYPT1 (Thr696) antibody, which was in turn bound by a HRP-conjugated goat anti–rabbit IgG secondary antibody. Colorimetric reaction was performed according to the manufacturer's procedures and detected by absorbance measurement at 450-nm wavelength.

Fluorescent staining and confocal microscopy

Cells were transfected with mCherry-MRCKα constructs and, after 16 h, fixed with 3.7% PFA, permeabilized for 10 min in PBS 0.1% Triton X-100 (Sigma-Aldrich), and saturated in 10% donkey serum (Sigma-Aldrich). Cells were stained with Phallodin-Atto 488 (Sigma-Aldrich) and immunostained for pS19MLC2 and pT18/S19MLC2, using as secondary antibody anti-rabbit Alexa Fluor 405 (Thermo Fisher Scientific) or anti-rabbit Alexa Fluor 647 (Sigma-Aldrich). After staining, samples were mounted in Mowiol 4-88 (Sigma-Aldrich). Images were acquired at room temperature with a confocal laser-scanning microscope (SPEII DM5500 CSQ; Leica) equipped with a 63×/1.30 HCX Plan-Apochromat oil-immersion objective lens (ACS APO 63×/1.30 oil CS 0.17/E, 0.16) using Leica LAS AF software.

STED nanoscopy

Cells transfected with GFP-MRCKα 1–478 for 16 h were fixed with 3.7% PFA, permeabilized for 10 min in PBS 0.1% Triton X-100 (Sigma-Aldrich), and saturated in 10% donkey serum (Sigma-Aldrich). Then cells were stained with Phallodin-Atto 594 (Sigma-Aldrich) and immunostained using secondary antibody conjugated with Atto647N (Sigma-Aldrich). After staining, samples were mounted in Mowiol 4-88. Images were acquired at room temperature with a custom STED microscope (Galiani et al., 2012; Bianchini et al., 2015) equipped with a pulsed supercontinuum laser ALP-710-745-SC (Fianium), which delivers both the excitation (566 and 640 nm) and the depletion (715 and 745 nm) beams. The STED beams can be engineered in a user-adjustable combination of doughnut and bottle shapes so that both 2D and 3D superresolution can be achieved. The imaging parameters used for the images presented are as follows: pixel size 20, 20, and 80 nm (x, y, and z respectively); pixel dwell time 0.5 ms; excitation power at 566 nm 12 µW; doughnut STED beam power 14 mW; bottle STED beam power 9 mW; laser repetition rate 20 MHz; fluorescence detection band 570–640 nm; and objective lens 100× Leica HCX PL APO CS 1.4 oil.

Live microscopy experiments

Time-lapse confocal experiments were performed by means of SP8 confocal microscope (Leica), equipped with 63× (HC PL APO CS2 63×/1.40 oil) and 100× (HC PL APO CS2 100×/1.40 oil) objectives, 37°C humidified chamber with 5% CO$_2$, and hybrid detectors. Deconvolution of time-lapse 3D stacks was performed by Huygens Professional software. All the live microscopy experiments were conducted in confluent MCF10A or MDCK epithelia, except for the experiment in which we needed flattened cells to study iEAAR bundle network dynamics (see Actin bleaching experiments section).

Actin bleaching experiments

MCF10A cells were cotransfected with pEGFP-Actin (Clontech) and mCherry-MRCKα 1–478. When myosin inhibition was required, cells

were treated with 100 µM blebbistatin starting 10 min before bleaching. We performed these experiments in subconfluence conditions, where the iEAAR bundle network triggered by mCherry-MRCKα 1–478 is more extended, with longer bundles and parallel to the bottom glass. Cells were visualized by means of confocal laser-scanning microscope (TCS SP2 with DM IRE2; Leica) equipped with a 63×/1.40 HCX Plan-Apochromat oil-immersion objective. Bleaching experiments were performed by enlightening regions corresponding to actin fibers or EAARs using 1–10 iterations with an Ar/ArKr laser at 488-nm wavelength set at the maximum power. Before and after bleaching, EGFP-actin structures were visualized using the same laser set at 10–20% power. After-bleaching time-lapse acquisition was performed using a frame rate of 15–30 s. Unwanted time-dependent whole-field bleaching was corrected by using a bleach correction plugin for ImageJ (Miura et al., 2014).

Drug-induced EAAR/actin-cables collapse

To investigate the role of actin polymerization on iEAAR dynamics, subconfluent MCF10A cells were cotransfected with pEGFP-Actin (Clontech) and mCherry-MRCKα 1–478. After the expression of the exogenous proteins, cells were treated with 1 µM latrunculin A or 3 µM cytochalasin D. In addition, blebbistatin and cytochalasin D cotreatment was performed as follows. After 100 µM blebbistatin pretreatment for 10 min, medium was renewed with a solution containing 100 µM blebbistatin and 3 µM cytochalasin D. Cells were imaged by means of a Leica SP8 confocal microscope, equipped with 63× (HC PL APO CS2 63×/1.40 OIL) objective, 37°C humidified chamber with 5% CO_2, and hybrid detectors with a time frame of 20 s. Lengths of bundles were manually measured with ImageJ software. The shortening rate (SR) was calculated using the following formula: $SR = [L(t + dt) - L(t)]/dt$, where L is the overall length of the bundle, t is a given time, and dt is the interval of time between consecutive frames.

Image analysis

The radial actin profile of aEAAR and iEAAR was measured by means of a custom-written image analysis Matlab script. To measure the mean radial profile, we analyzed images in the following way. The center of the EAAR was identified, and the fluorescence profile for each line going through the center was measured on each image, as a function of the angle. A radial profile was obtained by taking the mean of the angles. All profiles were then rescaled by their maximum and the mean taken to obtain a mean profile. The distribution of ring size was measured by computing the distribution of the distance where the maximum fluorescence would occur and the distance at which fluorescence would halve.

To measure the extensibility of the actin cables, we photobleached the cables in a dashed pattern and evaluated the length of the dashed regions by means of image analysis techniques. A line region of interest (ROI) was drawn on the filament at the first frame, and particle image velocimetry algorithms were used to move the ROI during the video, to follow even the slight movement of the cable and the retracting cell. At each time point, an 8-pixel-wide strip was superimposed on the ROI to measure the linear fluorescence profile, obtained by taking the maximum intensity in each column of the ROI. The obtained profile was then a chainsaw-like profile. The space coordinate corresponding to half the valley-to-peak intensity was taken as the reference for the edge of each dash. To measure the length, the difference between each of the coordinates was taken. To determine the speed of the bundle, the autocorrelation of the same fluorescence profile was used.

To measure fluorescence recovery intensity of the iEAAR, the photobleached region was identified and tracked over time, taking into account the cell movement during the assay. The total intensity measured within the ROI was corrected with the ratio between the fluorescence of the cell (minus the ROI) at the beginning and that at each particular time point, to consider bleaching induced by illumination. As a measure of recovery, we used the difference between corrected intensities at time t and immediately after the bleaching, divided by the difference between pre- and postbleaching.

Statistical analysis

All data are represented as the mean value of at least three experimental replicates. Error bars give SD or SEM as indicated in figure legends. When relevant, the number of samples (n) has been indicated in the figure. Statistical analysis was performed using GraphPad Prism software. Statistical significance was determined by Student's t test or one-way analysis of variance, with $P < 0.05$ considered significant.

Online supplemental material

Online supplemental material contains additional time-lapse experiments showing aEAAR assembly and epithelial extrusion from confluent MCF10A and MDCK cells (Fig. S1); analysis of the possible involvement of the different members of Rho-associated kinases family (Fig. S2); additional experiments aimed at identifying the localization of caspase cleavage sites in MRCKα and MRCKβ (Fig. S3); the localization of these cleavage sites in relation to secondary structure prediction (Fig. S4); and additional experiments relative to Figs. 5, 6, 7, and 8 (Fig. S5). In addition, 10 videos show the observation of actomyosin dynamics events in EAAR assembly and epithelial extrusion (Videos 1, 2, 3, 4, and 5) and the study of iEAAR/bundle network dynamics (Videos 6, 7, 8, 9, and 10).

References

Bianchini, P., C. Peres, M. Oneto, S. Galiani, G. Vicidomini, and A. Diaspro. 2015. STED nanoscopy: A glimpse into the future. *Cell Tissue Res.* 360:143–150. https://doi.org/10.1007/s00441-015-2146-3

Black, R.A., S.R. Kronheim, J.E. Merriam, C.J. March, and T.P. Hopp. 1989. A pre-aspartate-specific protease from human leukocytes that cleaves pro-interleukin-1 beta. *J. Biol. Chem.* 264:5323–5326.

Brown, S.B., K. Bailey, and J. Savill. 1997. Actin is cleaved during constitutive apoptosis. *Biochem. J.* 323:233–237. https://doi.org/10.1042/bj3230233

Byun, Y., F. Chen, R. Chang, M. Trivedi, K.J. Green, and V.L. Cryns. 2001. Caspase cleavage of vimentin disrupts intermediate filaments and promotes apoptosis. *Cell Death Differ.* 8:443–450. https://doi.org/10.1038/sj.cdd.4400840

Chen, F., R. Chang, M. Trivedi, Y. Capetanaki, and V.L. Cryns. 2003. Caspase proteolysis of desmin produces a dominant-negative inhibitor of intermediate filaments and promotes apoptosis. *J. Biol. Chem.* 278:6848–6853. https://doi.org/10.1074/jbc.M212021200

Coleman, M.L., E.A. Sahai, M. Yeo, M. Bosch, A. Dewar, and M.F. Olson. 2001. Membrane blebbing during apoptosis results from caspase-mediated activation of ROCK I. *Nat. Cell Biol.* 3:339–345. https://doi.org/10.1038/35070009

Crawford, E.D., and J.A. Wells. 2011. Caspase substrates and cellular remodeling. *Annu. Rev. Biochem.* 80:1055–1087. https://doi.org/10.1146/annurev-biochem-061809-121639

Crawford, E.D., J.E. Seaman, A.E. Barber II, D.C. David, P.C. Babbitt, A.L. Burlingame, and J.A. Wells. 2012. Conservation of caspase substrates across metazoans suggests hierarchical importance of signaling pathways over specific targets and cleavage site motifs in apoptosis. *Cell Death Differ.* 19:2040–2048. https://doi.org/10.1038/cdd.2012.99

Croft, D.R., M.L. Coleman, S. Li, D. Robertson, T. Sullivan, C.L. Stewart, and M.F. Olson. 2005. Actin-myosin-based contraction is responsible for apoptotic nuclear disintegration. *J. Cell Biol.* 168:245–255. https://doi.org/10.1083/jcb.200409049

Cullen, S.P., and S.J. Martin. 2009. Caspase activation pathways: Some recent progress. *Cell Death Differ.* 16:935–938. https://doi.org/10.1038/cdd.2009.59

Debnath, J., S.K. Muthuswamy, and J.S. Brugge. 2003. Morphogenesis and oncogenesis of MCF-10A mammary epithelial acini grown in three-dimensional basement membrane cultures. *Methods.* 30:256–268. https://doi.org/10.1016/S1046-2023(03)00032-X

Desouza, M., P.W. Gunning, and J.R. Stehn. 2012. The actin cytoskeleton as a sensor and mediator of apoptosis. *Bioarchitecture.* 2:75–87. https://doi.org/10.4161/bioa.20975

Elmore, S. 2007. Apoptosis: A review of programmed cell death. *Toxicol. Pathol.* 35:495–516. https://doi.org/10.1080/01926230701320337

Fu, S.C., K. Imai, T. Sawasaki, and K. Tomii. 2014. ScreenCap3: Improving prediction of caspase-3 cleavage sites using experimentally verified noncleavage sites. *Proteomics.* 14:2042–2046. https://doi.org/10.1002/pmic.201400002

Gagliardi, P.A., L. di Blasio, F. Orso, G. Seano, R. Sessa, D. Taverna, F. Bussolino, and L. Primo. 2012. 3-Phosphoinositide-dependent kinase 1 controls breast tumor growth in a kinase-dependent but Akt-independent manner. *Neoplasia.* 14:719–731. https://doi.org/10.1593/neo.12856

Gagliardi, P.A., L. di Blasio, A. Puliafito, G. Seano, R. Sessa, F. Chianale, T. Leung, F. Bussolino, and L. Primo. 2014. PDK1-mediated activation of MRCKα regulates directional cell migration and lamellipodia retraction. *J. Cell Biol.* 206:415–434. https://doi.org/10.1083/jcb.201312090

Gagliardi, P.A., A. Puliafito, L. di Blasio, F. Chianale, D. Somale, G. Seano, F. Bussolino, and L. Primo. 2015. Real-time monitoring of cell protrusion dynamics by impedance responses. *Sci. Rep.* 5:10206. https://doi.org/10.1038/srep10206

Galiani, S., B. Harke, G. Vicidomini, G. Lignani, F. Benfenati, A. Diaspro, and P. Bianchini. 2012. Strategies to maximize the performance of a STED microscope. *Opt. Express.* 20:7362–7374. https://doi.org/10.1364/OE.20.007362

Garnier, J., J.F. Gibrat, and B. Robson. 1996. GOR method for predicting protein secondary structure from amino acid sequence. *Methods Enzymol.* 266:540–553. https://doi.org/10.1016/S0076-6879(96)66034-0

Gomes, E.R., S. Jani, and G.G. Gundersen. 2005. Nuclear movement regulated by Cdc42, MRCK, myosin, and actin flow establishes MTOC polarization in migrating cells. *Cell.* 121:451–463. https://doi.org/10.1016/j.cell.2005.02.022

Gu, Y., T. Forostyan, R. Sabbadini, and J. Rosenblatt. 2011. Epithelial cell extrusion requires the sphingosine-1-phosphate receptor 2 pathway. *J. Cell Biol.* 193:667–676. https://doi.org/10.1083/jcb.201010075

Hirata, H., H. Tatsumi, and M. Sokabe. 2008. Mechanical forces facilitate actin polymerization at focal adhesions in a zyxin-dependent manner. *J. Cell Sci.* 121:2795–2804. https://doi.org/10.1242/jcs.030320

Kothakota, S., T. Azuma, C. Reinhard, A. Klippel, J. Tang, K. Chu, T.J. McGarry, M.W. Kirschner, K. Koths, D.J. Kwiatkowski, and L.T. Williams. 1997. Caspase-3-generated fragment of gelsolin: Effector of morphological change in apoptosis. *Science.* 278:294–298. https://doi.org/10.1126/science.278.5336.294

Kuipers, D., A. Mehonic, M. Kajita, L. Peter, Y. Fujita, T. Duke, G. Charras, and J.E. Gale. 2014. Epithelial repair is a two-stage process driven first by dying cells and then by their neighbours. *J. Cell Sci.* 127:1229–1241. https://doi.org/10.1242/jcs.138289

Lee, I.C., T. Leung, and I. Tan. 2014. Adaptor protein LRAP25 mediates myotonic dystrophy kinase-related Cdc42-binding kinase (MRCK) regulation of LIMK1 protein in lamellipodial F-actin dynamics. *J. Biol. Chem.* 289:26989–27003. https://doi.org/10.1074/jbc.M114.588079

Leung, T., X.Q. Chen, I. Tan, E. Manser, and L. Lim. 1998. Myotonic dystrophy kinase-related Cdc42-binding kinase acts as a Cdc42 effector in promoting cytoskeletal reorganization. *Mol. Cell. Biol.* 18:130–140. https://doi.org/10.1128/MCB.18.1.130

Lubkov, V., and D. Bar-Sagi. 2014. E-cadherin-mediated cell coupling is required for apoptotic cell extrusion. *Curr. Biol.* 24:868–874. https://doi.org/10.1016/j.cub.2014.02.057

Macara, I.G., R. Guyer, G. Richardson, Y. Huo, and S.M. Ahmed. 2014. Epithelial homeostasis. *Curr. Biol.* 24:R815–R825. https://doi.org/10.1016/j.cub.2014.06.068

Marston, D.J., C.D. Higgins, K.A. Peters, T.D. Cupp, D.J. Dickinson, A.M. Pani, R.P. Moore, A.H. Cox, D.P. Kiehart, and B. Goldstein. 2016. MRCK-1 drives apical constriction in C. elegans by linking developmental patterning to force generation. *Curr. Biol.* 26:2079–2089. https://doi.org/10.1016/j.cub.2016.06.010

Martin, A.C., and B. Goldstein. 2014. Apical constriction: Themes and variations on a cellular mechanism driving morphogenesis. *Development.* 141:1987–1998. https://doi.org/10.1242/dev.102228

Mashima, T., M. Naito, and T. Tsuruo. 1999. Caspase-mediated cleavage of cytoskeletal actin plays a positive role in the process of morphological apoptosis. *Oncogene.* 18:2423–2430. https://doi.org/10.1038/sj.onc.1202558

Michael, M., J.C.M. Meiring, B.R. Acharya, D.R. Matthews, S. Verma, S.P. Han, M.M. Hill, R.G. Parton, G.A. Gomez, and A.S. Yap. 2016. Coronin 1B reorganizes the architecture of F-actin networks for contractility at steady-state and apoptotic adherens junctions. *Dev. Cell.* 37:58–71. https://doi.org/10.1016/j.devcel.2016.03.008

Miura, K., C. Rueden, M. Hiner, J. Schindelin, and J. Rietdorf. 2014. ImageJ Plugin CorrectBleach V2.0.2. Zenodo. 10.5281/zenodo.30769

Núñez, R., S.M. Sancho-Martínez, J.M. Novoa, and F.J. López-Hernández. 2010. Apoptotic volume decrease as a geometric determinant for cell dismantling into apoptotic bodies. *Cell Death Differ.* 17:1665–1671. https://doi.org/10.1038/cdd.2010.96

Oropesa-Ávila, M., A. Fernández-Vega, M. de la Mata, J.G. Maraver, M.D. Cordero, D. Cotán, M. de Miguel, C.P. Calero, M.V. Paz, A.D. Pavón, et al. 2013. Apoptotic microtubules delimit an active caspase free area in the cellular cortex during the execution phase of apoptosis. *Cell Death Dis.* 4:e527. https://doi.org/10.1038/cddis.2013.58

Pearce, L.R., D. Komander, and D.R. Alessi. 2010. The nuts and bolts of AGC protein kinases. *Nat. Rev. Mol. Cell Biol.* 11:9–22. https://doi.org/10.1038/nrm2822

Petrache, I., K. Birukov, A.L. Zaiman, M.T. Crow, H. Deng, R. Wadgaonkar, L.H. Romer, and J.G. Garcia. 2003. Caspase-dependent cleavage of myosin light chain kinase (MLCK) is involved in TNF-alpha-mediated bovine pulmonary endothelial cell apoptosis. *FASEB J.* 17:407–416. https://doi.org/10.1096/fj.02-0672com

Rao, M.V., and R. Zaidel-Bar. 2016. Formin-mediated actin polymerization at cell-cell junctions stabilizes E-cadherin and maintains monolayer integrity during wound repair. *Mol. Biol. Cell.* 27:2844–2856. https://doi.org/10.1091/mbc.E16-06-0429

Rao, L., D. Perez, and E. White. 1996. Lamin proteolysis facilitates nuclear events during apoptosis. *J. Cell Biol.* 135:1441–1455. https://doi.org/10.1083/jcb.135.6.1441

Rice, R.L., D.G. Tang, and J.D. Taylor. 1998. Actin cleavage in various tumor cells is not a critical requirement for executing apoptosis. *Pathol. Oncol. Res.* 4:135–145. https://doi.org/10.1007/BF02904708

Rosenblatt, J., M.C. Raff, and L.P. Cramer. 2001. An epithelial cell destined for apoptosis signals its neighbors to extrude it by an actin- and myosin-dependent mechanism. *Curr. Biol.* 11:1847–1857. https://doi.org/10.1016/S0960-9822(01)00587-5

Sarbassov, D.D., D.A. Guertin, S.M. Ali, and D.M. Sabatini. 2005. Phosphorylation and regulation of Akt/PKB by the rictor-mTOR complex. *Science.* 307:1098–1101. https://doi.org/10.1126/science.1106148

Sebbagh, M., C. Renvoizé, J. Hamelin, N. Riché, J. Bertoglio, and J. Bréard. 2001. Caspase-3-mediated cleavage of ROCK I induces MLC phosphorylation and apoptotic membrane blebbing. *Nat. Cell Biol.* 3:346–352. https://doi.org/10.1038/35070019

Sebbagh, M., J. Hamelin, J. Bertoglio, E. Solary, and J. Bréard. 2005. Direct cleavage of ROCK II by granzyme B induces target cell membrane blebbing in a caspase-independent manner. *J. Exp. Med.* 201:465–471. https://doi.org/10.1084/jem.20031877

Swanger, S.A., A.L. Mattheyses, E.G. Gentry, and J.H. Herskowitz. 2016. ROCK1 and ROCK2 inhibition alters dendritic spine morphology in hippocampal neurons. *Cell. Logist.* 5:e1133266. https://doi.org/10.1080/21592799.2015.1133266

Tan, I., K.T. Seow, L. Lim, and T. Leung. 2001. Intermolecular and intramolecular interactions regulate catalytic activity of myotonic dystrophy kinase-related Cdc42-binding kinase alpha. *Mol. Cell. Biol.* 21:2767–2778. https://doi.org/10.1128/MCB.21.8.2767-2778.2001

Tan, I., J. Yong, J.M. Dong, L. Lim, and T. Leung. 2008. A tripartite complex containing MRCK modulates lamellar actomyosin retrograde flow. *Cell.* 135:123–136. https://doi.org/10.1016/j.cell.2008.09.018

Wickman, G.R., L. Julian, K. Mardilovich, S. Schumacher, J. Munro, N. Rath, S.A. Zander, A. Mleczak, D. Sumpton, N. Morrice, et al. 2013. Blebs produced by actin-myosin contraction during apoptosis release damage-associated molecular pattern proteins before secondary necrosis occurs. *Cell Death Differ.* 20:1293–1305. https://doi.org/10.1038/cdd.2013.69

Wu, S.K., A.K. Lagendijk, B.M. Hogan, G.A. Gomez, and A.S. Yap. 2015. Active contractility at E-cadherin junctions and its implications for cell extrusion in cancer. *Cell Cycle.* 14:315–322. https://doi.org/10.4161/15384101.2014.989127